CHAPTER 1

Visual Perception of Effervescence in Champagne and Other Sparkling Beverages

Gérard Liger-Belair[*,†,1]

Contents

* Groupe de Spectrométrie Moléculaire et Atmosphérique, UMR CNRS 6089, UFR Sciences Exactes et Naturelles, BP 1039, 51687 Reims Cedex 2, France
† Laboratoire d'Œnologie et Chimie Appliquée, Unité de Recherche sur la Vigne et le Vin de Champagne (URVVC), Université de Reims Champagne-Ardenne, Reims Cedex 2, France
[1] Corresponding author: Gérard Liger-Belair, *E-mail address:* gerard.liger-belair@univ-reims.fr

Advances in Food and Nutrition Research, Volume 61
ISSN 1043-4526, DOI: 10.1016/S1043-4526(10)61001-7

Abstract

The so-called *effervescence* process, which enlivens champagne, sparkling wines, beers, and carbonated beverages in general, is the result of the fine interplay between CO_2-dissolved gas molecules, tiny air pockets trapped within microscopic particles during the pouring process, and some liquid properties. This chapter summarizes recent advances obtained during the last decade concerning the physicochemical processes behind the nucleation, rise, and burst of bubbles found in glasses poured with sparkling beverages. Those phenomena observed in close-up through high-speed photography are often visually appealing. Moreover, the kinetics of gas discharging from freshly poured glasses was monitored with time, whether champagne is served into a flute or into a coupe. The role of temperature was also examined. We hope that your enjoyment of champagne will be enhanced after reading this fully illustrated review dedicated to the deep beauties of nature often hidden behind many everyday phenomena.

I. INTRODUCTION

From a strictly chemical point of view, Champagne and other sparkling wines are multicomponent hydroalcoholic systems supersaturated with CO_2-dissolved gas molecules, formed during the second, alcoholic, fermentation process (Liger-Belair, 2002, 2003, 2004). As soon as a bottle of champagne or sparkling wine is uncorked, the progressive release of CO_2-dissolved gas molecules is responsible for bubble formation, the so-called effervescence process. It is worth noting that approximately 5 L of CO_2 must escape from a typical 0.75 L champagne bottle. To get an idea of how many bubbles are potentially involved all along the degassing process from this single bottle, we can divide this volume of CO_2 to be released by the average volume of a typical bubble of 0.5 mm in diameter. A huge number close to 10^8 is found. Actually, champagne and other sparkling wine tasting mainly differs from still noneffervescent wine tasting due to the presence of those myriad of bubbles continuously

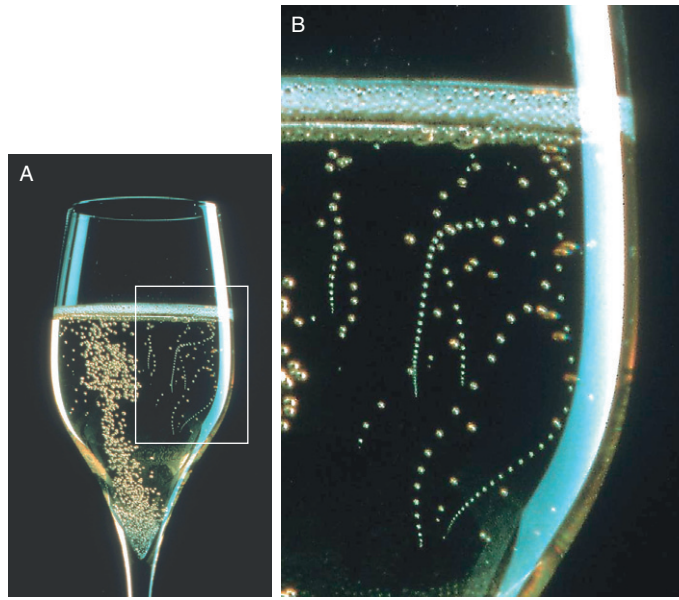

FIGURE 1.1 Photograph of a typical flute poured with champagne (A), and close-up on particles acting as bubble nucleation sites freely floating in the bulk of the flute, thus creating lovely bubble trains in motion in the champagne bulk (B) (©Alain Cornu/ Collection CIVC).

rising through the liquid medium. This is the reason why considerable efforts have been conducted in the last few years in order to better illustrate, detect, understand, and finally control each and every parameter involved in the bubbling process. Without bubbles, champagne and other sparkling wines would be unrecognizable as such (see Fig. 1.1), but the role of effervescence goes far beyond the sole esthetical point of view. This chapter covers recent progress in the field of champagne science.

II. WITHIN A CHAMPAGNE BOTTLE

A. Where do CO_2 molecules dissolved in champagne come from?

The modern production of champagne is not so far removed from that empirically developed by the Benedictine monk Dom Pierre Pérignon in the late seventeenth century. This method is also used outside

the Champagne region. Sparkling wines produced as such are labeled *méthode traditionelle*. Indeed, most American and Australian sparkling winemakers use this method to elaborate their own sparkling wines. This method involves several distinct steps.

1. A first alcoholic fermentation

Three grape cultivars are grown in the 75,000 acres of the Champagne vineyards: *Chardonnay* (a white grape), *Pinot Meunier*, and *Pinot Noir* (both dark grapes). Usually around mid-september, the grapes harvested from these vineyards are pressed to make a juice, called ''the grape must.'' After pressing, the must is transferred into an open vat where yeast (*Saccharomyces cerevisiae*) is added. Generally speaking, the key metabolic process during winemaking is alcoholic fermentation: the conversion of sugars into ethanol and carbon dioxide by yeast. The process of fermentation was first scientifically described by the French chemist Joseph-Louis Gay Lussac, in 1810, when he demonstrated that glucose is the basic starting block for producing ethanol:

$$C_6H_{12}O_6 \rightarrow 2CH_3CH_2OH + 2CO_2 \quad (1)$$

The manner in which yeast contributes to the fermentation process was not clearly understood until 1857, when the French microbiologist Louis Pasteur discovered that not only does the fermentation process *require* any oxygen, but also alcohol yield is actually *reduced* by its presence. The amount of ethanol generated by this first alcoholic fermentation is about 11%. At this step, ''champagne'' is still actually a noneffervescent white wine, because the carbon dioxide produced during the first alcoholic fermentation is allowed to escape into the atmosphere.

2. The art of blending

Because it is rare that a single wine of a single vintage from a single vineyard and grape variety will provide the perfect balance of flavor, sugar level, and acidity necessary for making a fine champagne, wine makers will often mix several different still wines. This is called the *assemblage* (or blending) step, and it is carried out directly after the first alcoholic fermentation is complete. Blending is considered a key step in the art of champagne-making. A cellar master will sometimes blend up to 80 different wines from various grape varieties, vineyards, and vintages to produce one champagne. The blending of still wines originally made from the three grape cultivars forms a base wine, which will then undergo a second fermentation—the key step in producing the ''sparkle'' in champagne and other sparkling wines.

3. The *prise de mousse*: A second alcoholic fermentation

Once the base wine is created, sugar (about 24 g/L) and yeast are added. The entire concoction is put into thick-walled glass bottles and sealed with caps. The bottles are then placed in a cool cellar (12–14°C), and the wine is allowed to slowly ferment for a second time, producing alcohol and carbon dioxide again. Actually, during this second fermentation process which occurs in cool cellars, the bottles are sealed, so that the CO_2 molecules cannot escape and progressively dissolve into the wine. Therefore, CO_2-dissolved molecules into the wine and gaseous CO_2 molecules under the cork progressively establish equilibrium—an application of Henry's law which states that the partial pressure of a given gas above a solution is proportional to the concentration of the gas dissolved into the solution, as expressed by the following relation:

$$c = k_{\mathrm{H}} P_{\mathrm{CO_2}} \tag{2}$$

where c is the concentration of dissolved CO_2 molecules, $P_{\mathrm{CO_2}}$ is the partial pressure of CO_2 molecules in the vapor phase, and k_{H} is the Henry's law constant. For a given gas, k_{H} is strongly temperature dependent. The lower the temperature, the higher the Henry's law constant, and therefore the higher the solubility.

In champagne and other sparkling wines, Agabaliantz thoroughly examined the solubility of dissolved CO_2 molecules as a function of both temperature and wine parameters (Agabaliantz, 1963). His empirical relationships are still in use nowadays by champagne and other sparkling winemakers. For a typical sparkling wine elaborated according to the *méthode traditionnelle*, Agabaliantz established the temperature dependence of the Henry's law constant, which is displayed in Table 1.1.

Thermodynamically speaking, the behavior of Henry's law constant as a function of temperature can be conveniently expressed with a Van't Hoff like equation as follows:

$$k_{\mathrm{H}}(\theta) = k_{298\,\mathrm{K}} \exp\left[-\frac{\Delta H_{\mathrm{diss}}}{\mathfrak{R}}\left(\frac{1}{\theta} - \frac{1}{298}\right)\right] \tag{3}$$

where ΔH_{diss} is the dissolution enthalpy of CO_2 molecules in the liquid medium (in J/mol), $\mathfrak{R}$ is the ideal gas constant (8.31 J/K/mol), and θ is the absolute temperature (in K). By fitting Agabaliantz data with the latter equation, it is worth noting that the dissolution enthalpy of CO_2 molecules in champagne may be evaluated (Liger-Belair, 2005). The best fit to Agabaliantz data was found with $\Delta H_{\mathrm{diss}} \approx 24{,}800$ J/mol (see Fig. 1.2). In comparison, the dissolution enthalpy of CO_2 molecules in pure water is about 19,900 J/mol (Lide and Frederikse, 1995).

TABLE 1.1 Henry's law constant of CO_2 in champagne as a function of temperature, for a typical champagne with 12.5% (v/v) of ethanol and 10 g/L of sugars

Temperature (°C)	Henry's law constant k_H (kg/m^3/atm)
0	2.98
1	2.88
2	2.78
3	2.68
4	2.59
5	2.49
6	2.41
7	2.32
8	2.23
9	2.16
10	2.07
11	2.00
12	1.93
13	1.86
14	1.79
15	1.73
16	1.67
17	1.60
18	1.54
19	1.48
20	1.44
21	1.40
22	1.34
23	1.29
24	1.25
25	1.21

Compiled from the data by Agabaliantz (1963).

B. The pressure under the cork

Following Eq. (1), 24 g/L of sugar added in closed bottles to promote the second alcoholic fermentation produces approximately 11.8 g/L of CO_2 within each bottle. Therefore, a typical 75-cl champagne bottle contains close to 9 g of CO_2 molecules. By use of the molar mass of CO_2 (44 g/mol), and the molar volume of an ideal gas (close to 24 L/mol at 12 °C), it can be deduced that about 5 L of gaseous CO_2 is trapped into a single bottle of champagne (i.e., six times its own volume!).

Because the solubility of CO_2 strongly depends on the champagne temperature, the pressure of gaseous CO_2 under the cork also strongly

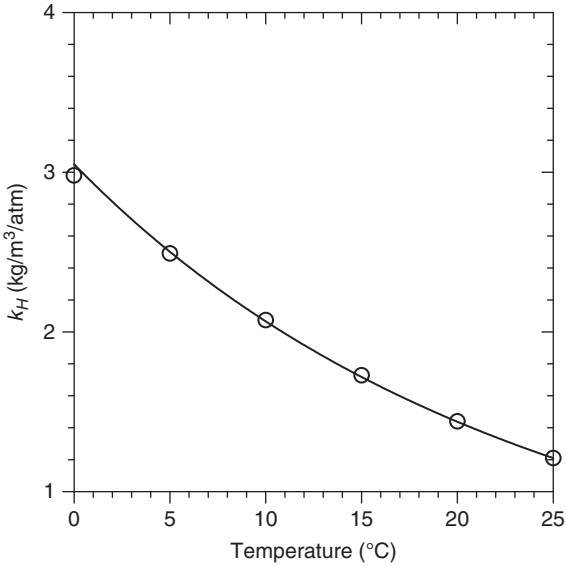

FIGURE 1.2 Henry's law constant as a function of temperature (O) (redrawn from Agabaliantz data); the dashed line is the best fit to Agabaliantz data, drawn with the Van't Hoff like Eq. (3) and with $\Delta H_{\text{diss}} \approx 24{,}800$ J/mol.

depends, in turn, on the champagne temperature. The physicochemical equilibrium of CO_2 molecules within a champagne bottle is ruled by both Henry's law (for CO_2-dissolved gas molecules) and the ideal gas law (for the gaseous CO_2 in the headspace under the cork). Moreover, the conservation of the total mass of CO_2 molecules (dissolved into the wine and in the vapor phase under the cork) applies, since bottles are hermetically closed. Therefore, by combining the two aforementioned laws with mass conservation, the following relationship can easily be determined which links the pressure P of gaseous CO_2 under the cork (in bars) with both temperature and the bottle's parameters as

$$P \approx \frac{m\mathfrak{R}\theta}{4.4 \times 10^3 v + (k_{\text{H}}\mathfrak{R}\theta)V} \tag{4}$$

where m is the total mass of CO_2 within the bottle (in g), θ the champagne temperature (in K), $\mathfrak{R}$ the ideal gas constant (8.31 J/K/mol), k_{H} the Henry's law constant given in Table 1.1 (in g/L/bar), V volume of champagne within the bottle (in L), and v is the volume of the gaseous headspace under the cork (in L).

For a typical champagne bottle with $V = 75$ cl, a volume in the headspace of $v = 25$ mL, and a total mass of CO_2 trapped within the bottle of

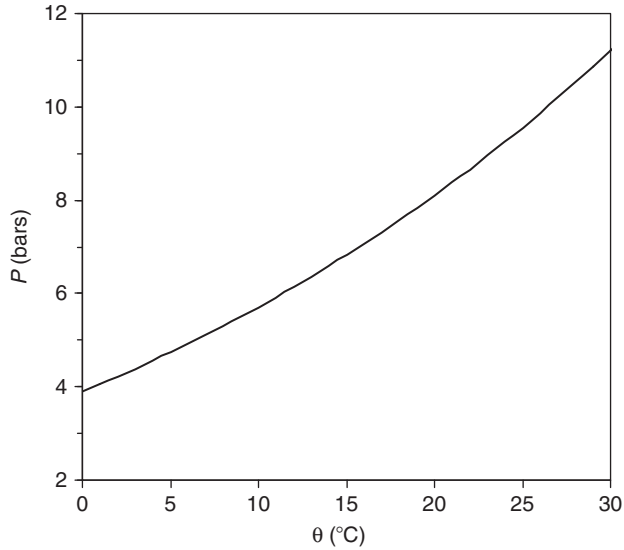

FIGURE 1.3 Pressure of gaseous CO_2 under the cork of a typical 75 cl champagne bottle as a function of champagne temperature.

$m = 9$ g, the variation of the pressure P under the cork with the champagne temperature θ is displayed in Fig. 1.3. At the temperature of champagne tasting (usually between 8 and 10 °C), the pressure within a typical 75 cl champagne bottle is close to 5 bars (i.e., 5×10^5 N/m^2).

C. The chemical composition of champagne

From the point of view of the chemist, champagne can indeed be viewed as a multicomponent aqueous solution. The chemical composition of a typical Champagne wine is reported in Table 1.2 (Dussaud, 1993).

Typically, gases like CO_2 undergo specific reactions with water. Equilibrium is established between the dissolved $(CO_2)_{aq}$ and H_2CO_3, the carbonic acid:

$$(CO_2)_{aq} + H_2O \leftrightarrow H_2CO_3 \tag{5}$$

Moreover, carbonic acid is a weak acid that dissociates in two steps:

$$H_2CO_3 + H_2O \leftrightarrow H_3O^+ + HCO_3 \quad pK_{a1}\,(\text{at } 25\,^\circ\text{C}) = 6.37 \tag{6}$$

$$HCO_3^- + H_2O \leftrightarrow H_3O^+ + CO_3^{2-} \quad pK_{a2}(\text{at } 25\,^\circ\text{C}) = 10.25 \tag{7}$$

However, as the pH of champagne and other sparkling wines is relatively low (of order of 3.2), no carbonated species (CO_3^{2-}, HCO_3^-)

TABLE 1.2 Average composition of a typical Champagne wine (Dussaud, 1993)

Compound	Quantity
Ethanol	≈12.5 v/v%
CO_2	10–12 g/L
Glycerol	≈5 g/L
Tartaric acid	≈2.5–4 g/L
Lactic acid	≈4 g/L
Sugars	10–50 g/L
Proteins	5–10 mg/L
Polysaccharides	≈200 mg/L
Polyphenols	≈100 mg/L
Amino acids	0.8–2 mg/L
Volatile Organic Compounds (VOC)	≈700 mg/L
Lipids	≈10 mg/L
K^+	200–450 mg/L
Ca^{2+}	60–120 mg/L
Mg^{2+}	50–90 mg/L
SO_4^{2-}	≈200 mg/L
Cl^-	≈10 mg/L

Typically, pH ≈ 3.2 and the ionic strength is 0.02 M.

should coexist with dissolved CO_2. Recently, the ^{13}C Magnetic Resonance Spectroscopy (MRS) technique was used as an unintrusive and nondestructive method to determine the amount of CO_2 dissolved in closed bottles of Champagne and other sparkling wines (Autret *et al.*, 2005). Different well-separated peaks were recorded in a ^{13}C spectrum, as can be seen in Fig. 1.4: (i) the quadruplet of CH_3 group of ethanol appears at 17.9 ppm, (ii) the triplet of CH_2(–OH) group of ethanol at 57.3 ppm, and (iii) the singlet of CO_2 appears at 124.4 ppm, thus confirming the absence of other carbonated species (CO_3^{2-}, HCO_3^-) in the liquid matrix (contrary to fizzy waters, e.g., where pH values near neutrality enable the aforementioned carbonated species to cohabit with CO_2-dissolved gas molecules).

D. Uncorking the bottle

Have you ever thought about the velocity reached by an uncontrolled champagne cork popping out of a bottle? Measurements conducted in our laboratory in Reims led to typical velocities ranging from 50 to 60 km/h (Liger-Belair, 2009). When opening a bottle of champagne (or carbonated beverage in general), anyone has also already noticed the cloud of fog forming right above the bottle neck (as wonderfully illustrated by the photograph displayed in Fig. 1.5 taken by Jacques Honvault).

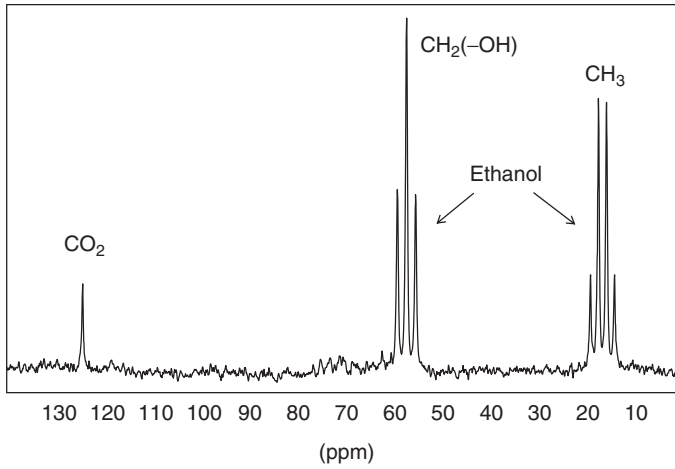

FIGURE 1.4 ^{13}C spectrum recorded to measure the CO_2 concentration in a typical Champagne wine (Autret *et al.*, 2005); it is clear that no carbonated species (CO_3^{2-}, HCO_3^-) coexist with dissolved CO_2.

FIGURE 1.5 Uncontrolled champagne cork popping out of a bottle; the cloud of fog forming right above the bottle neck clearly appears (©Jacques Honvault).

This cloud of fog is due to a significant drop in temperature in the headspace below the champagne surface, caused by the sudden gas expansion when the bottle is uncorked. Actually, this sudden temperature drop is responsible for the instantaneous condensation of water vapor into the form of this characteristic cloud of fog. Assuming an adiabatic expansion experienced by the gas volume of the headspace (from about 5 to 1 atm), the corresponding theoretical drop in temperature experienced by the gas volume may easily be accessed by the following and well-known relationship:

$$P^{(1-\Gamma)}\theta^{\Gamma} = \text{constant} \tag{8}$$

where P, θ, and Γ are the pressure, temperature, and ratio of specific heats of the gas volume experiencing adiabatic expansion, respectively. The ratio of specific heats for CO_2 molecules being 1.3, an adiabatic expansion from about 5–1 atm when uncorking the bottle corresponds to a theoretical drop in temperature close to 90 °C. No wonder, traces of water vapor immediately condensate into the form of a small cloud.

Moreover, in addition to this sudden temperature drop experienced by gases from the headspace, the fall of CO_2 partial pressure above the champagne surface linked with bottle uncorking leads to a huge consequence concerning the thermodynamic equilibrium of CO_2-dissolved molecules. Since the partial pressure of CO_2 falls above the champagne surface, the CO_2 dissolved in champagne is not in equilibrium any longer with its partial pressure in the vapor phase. Champagne enters a metastable state, that is, it contains CO_2 molecules in excess in comparison with what Henry's law states. To recover a new stable thermodynamic state corresponding to the partial pressure of CO_2 molecules in the atmosphere (about only 3.5×10^{-4} atm), almost all the carbon dioxide molecules dissolved into the champagne must escape. The champagne becomes supersaturated with CO_2. Before proceeding further, it is important to define the supersaturating ratio, used for quantifying CO_2 molecules in excess in a carbonated liquid. The supersaturating ratio S is defined as follows (Lubetkin and Blackwell, 1988):

$$S = \frac{c_L}{c_0} - 1 \tag{9}$$

where c_L is the concentration of CO_2 in the liquid bulk and c_0 is the equilibrium concentration of CO_2 corresponding to a partial pressure of gaseous CO_2 of 1 atm.

As soon as $S > 0$, a supersaturated liquid enters a metastable state and must degas to recover a supersaturating ratio equal to zero. In the case of Champagne wines, just after uncorking the bottle, c_L is the equilibrium concentration of CO_2 in the liquid bulk corresponding to a partial

pressure of CO_2 of about 5 atm. Because there is a strict proportionality between the concentration of dissolved CO_2 and its partial pressure in the vapor phase (as expressed by Henry's law), $c_L/c_0 \approx 5$. Therefore, just after uncorking the bottle, the supersaturating ratio of champagne is approximately $S \approx 4$, and champagne must degas. Actually, there are two mechanisms for gas loss: (i) losses due to diffusion through the surface of the liquid (invisible by the naked eye) and (ii) losses due to bubbling (the so-called effervescence process). But, how and where do all these bubbles form or *nucleate*?

III. THE BUBBLE NUCLEATION PROCESS

A. A critical radius required for bubble nucleation

Generally speaking, carbonated beverages are weakly supersaturated with CO_2-dissolved gas molecules. In weakly supersaturated liquids such as champagne and other sparkling wines, bubbles do not just pop into existence *ex nihilo*. Actually, to cluster into the form of bubbles, CO_2-dissolved gas molecules must cluster together and push their way through the liquid molecules that are held together by Van der Waals attractive forces. Bubble formation is therefore limited by an energy barrier (for a complete review, see the paper by Lugli and Zerbetto, 2007). This is the reason why in weakly supersaturated liquids, bubble formation and growing require preexisting gas cavities with radii of curvature large enough to overcome the nucleation energy barrier and grow freely (Lubetkin, 2003). This critical radius, denoted r^*, can easily be accessed by using standard thermodynamic arguments, or by using simple arguments based on classical diffusion principles (Liger-Belair and Rochard, 2008). The critical radius r^* of gas pockets required to enable bubble production in a carbonated beverage expresses as follows:

$$r^* \approx \frac{2\gamma}{P_0 S} \tag{10}$$

where γ is the surface tension of the liquid medium, of order of 50 mN/m in champagne and other sparkling wines (Dussaud, 1993), and P_0 is the atmospheric pressure ($P_0 \approx 10^5$ N/m^2). At the opening of a champagne bottle, because $S \approx 4$, the critical radius required to enable bubble nucleation is of the order of 0.25 μm.

Jones *et al.* (1999) made a classification of the broad range of nucleation likely to be encountered in liquids supersaturated with dissolved gas molecules (Jones *et al.*, 1999). Bubble formation from preexisting gas cavities larger than the critical size is referred to as nonclassical heterogeneous bubble nucleation (type IV bubble nucleation, following their

nomenclature). Generally speaking, effervescence in a glass of champagne or sparkling wine may have two distinct origins. It can be ''natural'' or ''artificial.''

B. "Natural" bubble nucleation

Natural effervescence is related to the bubbling process from a glass which has not experienced any specific surface treatment. Closer inspection of such glasses poured with champagne and other sparkling wines was conducted through a high-speed video camera fitted with a microscope objective (see the photograph displayed in Fig. 1.6). It revealed that most of the bubble nucleation sites were found to be located on preexisting gas cavities trapped inside hollow and roughly cylindrical cellulose–fiber-made structures on the order of 100-μm long with a cavity mouth of several micrometers (see Fig. 1.7) (Liger-Belair, 2002, 2003; Liger-Belair *et al.*, 2004).

The hollow cavity (a kind of tiny channel within the fibers) where a gas pocket is trapped during the pouring process is called the *lumen*. It can be clearly noticed from Fig. 1.7 that the radii of curvature of gas pockets trapped inside the fiber's lumen are much higher than the aforementioned critical radius r^*. Fibers probably adhere on the flute wall due to electrostatic forces (especially if the glass or the flute is vigorously wiped by a towel). Natural effervescence may also arise from tartrate crystals precipitated on the glass wall and resulting from the evaporation process after rinsing the glass with tap water. Therefore, there is a substantial variation concerning the ''natural'' effervescence between flutes depending on how the flute was cleaned and how and where it was left before serving.

FIGURE 1.6 High-speed video camera used to visualize bubble nucleation sites in a glass poured with champagne (photograph by Hubert Raguet).

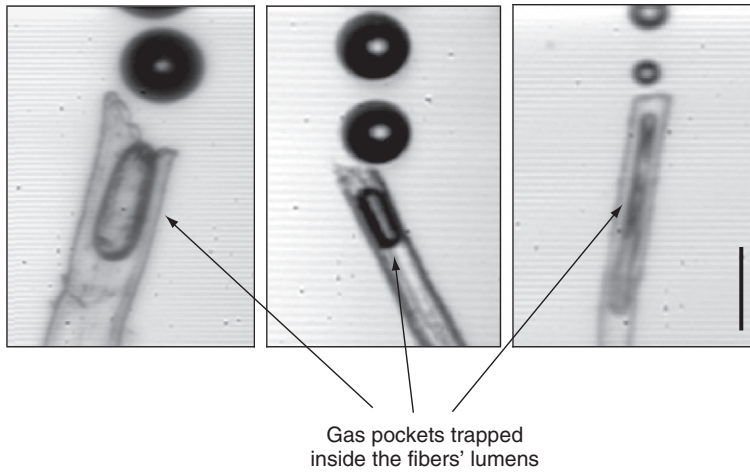

FIGURE 1.7 Three typical cellulose fibers adsorbed on the wall of a glass poured with champagne; the gas pockets trapped inside the fibers' lumen and responsible for bubble formation clearly appear (bar = 100 μm) (Photographs by Gérard Liger-Belair).

The mechanism of bubble release from a fiber's lumen has already been described in recent papers (Liger-Belair *et al.*, 2005b, 2006a). In very short, after opening a bottle of champagne or sparkling wine, the thermodynamic equilibrium of CO_2 molecules dissolved in the liquid medium is broken. CO_2-dissolved molecules become in excess in comparison with what the liquid medium can withstand. Therefore, CO_2 molecules will escape from the liquid medium through every available gas–liquid interface to reach a vapor phase. Actually, once the sparkling beverage is poured into a glass, the tiny air pockets trapped inside the collection of fibers adsorbed on the glass wall offer gas–liquid interfaces to CO_2-dissolved molecules, which cross the interface toward the gas pockets. In turn, gas pockets grow inside the fibers' lumen. When a gas pocket reaches the tip of a fiber, a bubble is ejected, but a portion of the gas pocket remains trapped inside the fiber's lumen, shrinks back to its initial position, and the cycle starts again until bubble production stops through lack of dissolved gas molecules (see the very typical time sequence displayed in Fig. 1.8).

C. Entrapping an air pocket within a fiber

Cellulose fibers are in the form of hollow tubes of several hundreds of micrometers long and with a cavity mouth of several micrometers wide. The fiber wall section consists of densely packed cellulose microfibrils, with a preferential orientation along the fiber axis. Cellulose microfibrils consist of glucose units bounded in a β-conformation favoring straight

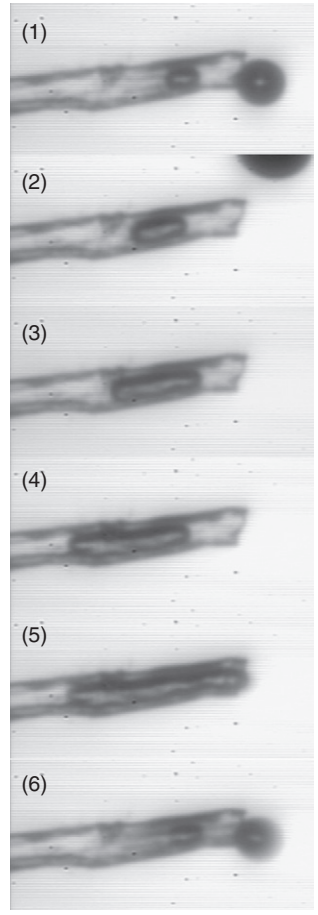

FIGURE 1.8 Time sequence illustrating one period of the cycle of bubble production from the lumen of a typical hollow cellulose fiber adsorbed on the wall of a glass poured with champagne; from Frame 1 to Frame 5, the time interval between successive frames is about 200 ms, but from Frame 5 to Frame 6, the time interval is only 1 ms (bar = 50 μm) (Photographs by Cédric Voisin and Gérard Liger-Belair).

polymer chains. The different structural levels of a cellulose fiber are presented in Fig. 1.9. For a current review on the molecular and supramolecular structures of cellulose, see the article by O'Sullivan and references therein (O'Sullivan, 1997).

From the physics point of view, cellulose fibers can indeed be considered as tiny roughly cylindrical capillary tubes of radius r and length h. Consequently, a wetting liquid placed into contact with this highly hydrophilic material penetrates it by capillary action. Actually, in capillaries with radii much smaller than the capillary length, gravity may be

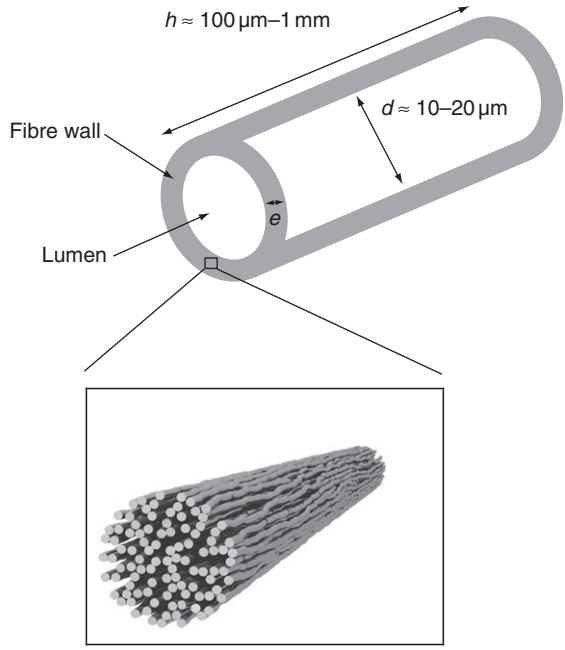

FIGURE 1.9 The different structural levels of a typical cellulose fiber; the fiber wall consists of closely packed cellulose microfibrils oriented mainly in the direction of the fiber.

neglected. Therefore, η being the viscosity of the liquid phase, γ being the surface tension of liquid, z being the distance of penetration at time t, and θ the effective contact angle between the liquid and the capillary wall, the overall balance of forces on the liquid in the capillary may be expressed as

$$\rho\left[z\frac{\mathrm{d}^2z}{\mathrm{d}t^2}+\left(\frac{\mathrm{d}z}{\mathrm{d}t}\right)^2\right]=\frac{2\gamma\cos\theta}{r}-\frac{8\eta z}{r^2}\frac{\mathrm{d}z}{\mathrm{d}t} \tag{11}$$

The left-hand side of the latter equation is related to the liquid inertia, whereas both terms in the right-hand side are related to capillarity (the driving force), and viscous resistance, respectively. Under steady conditions, capillarity is balanced by the viscous drag of the liquid, and the famous Lucas–Washburn's equation can be derived (De Gennes *et al.*, 2002):

$$z^2=\frac{r\gamma\cos\theta}{2\eta}t \tag{12}$$

Let us imagine a liquid edge spreading with a velocity v along a solid surface where cellulose fibers are adsorbed. This is basically what happens

when you fill a glass with a liquid. Actually, a liquid edge progressively advances along the vertical glass wall at a velocity v of order of several centimeter per second. As soon as the wetting liquid gets in touch with the fiber, some liquid progressively penetrates and fills the fiber's lumen by capillary rise. Finally, a gas pocket may be trapped within the fiber if the time τ taken by the liquid to completely fill the lumen by capillary action is greater than the characteristic time T taken by the liquid edge to completely submerge the fiber inside the liquid (see the scheme displayed in Fig. 1.10).

By retrieving Eq. (12) with the characteristic fiber's parameters defined in Fig. 1.10, the characteristic time required to completely fill the fiber's lumen by capillary action may be expressed as:

$$\tau = \frac{2\eta h^2}{r\gamma \cos\theta} \tag{13}$$

Considering a fiber with a length h, inclined by an angle α with regard to the liquid edge advancing over it at a velocity v, leads to the following time required for the fiber to be completely submerged:

$$T = \frac{h \sin\alpha}{v} \tag{14}$$

The condition of gas entrapment inside the fiber therefore expresses as $\tau > T$, that is,

$$\frac{2\eta h^2}{r\gamma \cos\theta} > \frac{h \sin\alpha}{v} \tag{15}$$

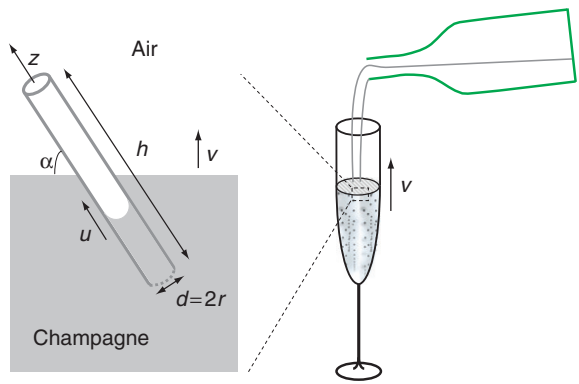

FIGURE 1.10 From the physics point of view, a fiber may be seen as a tiny capillary tube which gets invaded by a wetting liquid placed into contact with one of the fiber's tip; *v* is the velocity of the liquid edge advancing over the fiber, and *u* is the velocity at which the meniscus advances inside the fiber's lumen by capillary action (Liger-Belair *et al.*, 2005b).

Because cellulose is a highly hydrophilic material, the contact angle of an aqueous liquid on it is relatively small (about 30° with pure water). Consequently, $\cos\theta \approx 1$. Finally, the condition of entrapment may be rewritten as follows:

$$\frac{h}{r\sin\alpha} > \frac{\gamma}{2\eta v} \tag{16}$$

with the geometric parameters of the cellulose fiber lying on the left-hand side of Eq. (16) and the liquid parameters lying on the right-hand side of Eq. (16).

The entrapment of an air pocket inside the lumen of a fiber during the filling of a glass is therefore favored by the following conditions, depending on both fiber and liquid parameters: (i) as elongated fibers as possible (h long) (ii) of small lumen's radii r, (iii) fibers as horizontal as possible with regard to the liquid edge (i.e., sin α small), (iv) liquids with a small surface tension γ, (v) and a high viscosity η, and finally, (vi) a high velocity for the liquid edge advancing along the glass wall. It is worth noting that both conditions (iv) and (v) imply that hydroalcoholic carbonated beverages are more favorable than fizzy waters to entrap air pockets inside cellulose fibers during the pouring process. Actually, the surface tension of champagne and beer is of the order of 50 mN/m (i.e., about 20 mN/m less than the surface tension of pure water), and their dynamic viscosity is about 50% higher than that of pure water.

D. Modeling the repetitive bubble nucleation from a cellulose fiber

As seen in Fig. 1.8, the whole process leading to the production of a bubble from a cellulose fiber's tip can be coarsely divided in two main steps: (i) the growth of the gas pocket trapped inside the fiber's lumen (from frame 1 to frame 5) and (ii) the bubble detached as the gas pocket reaches the fiber's tip (from frame 5 to frame 6). Actually, it is clear from the numerous close-up time sequences taken with the high-speed video camera, that the time scale of the bubble detachment is always very small (≈1 ms) compared with the relatively slow growth of the gas pocket (several tens to several hundreds of meterseconds). Therefore, the whole cycle of bubble production seems to be largely governed by the growth of the gas pocket trapped inside the fiber's lumen. This tiny gas pocket was modeled as a slug-bubble growing trapped inside an ideal cylindrical microchannel and being fed with CO_2-dissolved molecules diffusing (i) directly from both ends of the gas pocket and (ii) through the fiber wall, which consists of closely packed cellulose microfibrils oriented mainly in the direction of the fiber (Liger-Belair *et al.*, 2004; Topgaard,

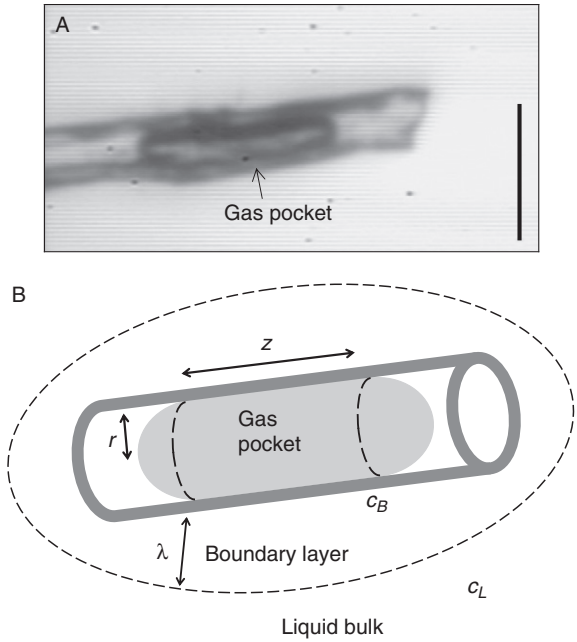

FIGURE 1.11 Real gas pocket trapped within the lumen of a cellulose fiber acting as a bubble nucleation site in a glass poured with champagne (A), modeled as a slug-bubble trapped inside an ideal cylindrical microchannel and being fed with CO_2-dissolved molecules diffusing, (i) directly from the liquid bulk through both ends of the gas pocket and (ii) through the wall of the microchannel (B) (bar = 50 μm).

2003). A scheme is displayed in Fig. 1.11, where the geometrical parameters of the tiny gas pocket growing by diffusion are defined.

Taking into account the diffusion of CO_2-dissolved molecules from the liquid bulk to the gas pocket, the growth of this gas pocket with time t was linked with both liquid and fiber parameters as follows (Liger-Belair *et al.*, 2005b):

$$\begin{cases} z(t) \approx (z_0 + A\tau)\exp(t/\tau) - A\tau \\ \text{with } \tau = \dfrac{(P + 2\gamma/r)r\lambda}{2\Re\theta D_\perp \Delta c} \quad \text{and} \quad A = \dfrac{4\Re\theta D_0 \Delta c}{(P + 2\gamma/r)\lambda} \end{cases} \tag{17}$$

where z is the length of the gas pocket, z_0 the initial length of the gas pocket before it starts its growth through the lumen, at each cycle of bubble production (see e.g., frame 1 and frame 6 in Fig. 1.8), P the ambient pressure, D_0 the diffusion coefficient of CO_2-dissolved molecules in the liquid bulk, $D_\perp$ the diffusion coefficient of CO_2-dissolved molecules through the fiber wall (and therefore perpendicular to the cellulose

microfibrils), $\Delta c = c_L - c_B = c_L - k_H P_B = c_L - k_H(P_0 + 2\gamma / r)$ the difference in CO_2-dissolved concentrations between the liquid bulk and the close vicinity of the gas pocket surface in equilibrium with the gaseous CO_2 in the gas pocket, and λ is the boundary layer thickness where a linear gradient of CO_2-dissolved concentration is assumed.

In the previous work, the transversal diffusion coefficient $D_\perp$ of CO_2 molecules through the fiber wall was approached and properly bounded by $D_\perp / D_0 \approx 0.1$ and $D_\perp / D_0 \approx 0.3$ (Liger-Belair *et al.*, 2004). For modeling purposes, an intermediate value of about $D_\perp \approx 0.2 D_0$ was proposed and will be used hereafter. The whole cycle of bubble production being largely governed by the growth of the gas pocket trapped inside the fiber's lumen, the period of bubble formation from a single cellulose fiber is therefore equal to the total time T required by the tiny gas pocket to grow from its initial length, denoted z_0, to its final length, denoted z_f, as it reaches the fiber's tip (see frame 5 in Fig. 1.8). By retrieving Eq. (17), it is therefore possible to access the frequency of bubble formation f (expressed in s^{-1}) from a single fiber as follows:

$$f \approx \frac{1}{T} \approx \frac{2\Re\theta D_\perp \Delta c}{r\lambda(P_0 + 2\gamma/r)\ln[(z_f + 10r)/(z_0 + 10r)]} \tag{18}$$

To go further on with the dependence of the bubbling frequency with both liquid and fiber parameters, we can replace in Eq. (18) the diffusion coefficient D_0 by its theoretical expression approached through the well-known Stokes–Einstein equation ($D_0 \approx k_B\theta\ /6\pi\eta d$), k_B being the Boltzman constant (1.38×10^{-23} J/K), and d being the characteristic size of the CO_2 molecule's hydrodynamic radius ($d \approx 10^{-10}$ m). By replacing in Eq. (18) each parameter by its theoretical expression and each constant by its numerical value, the variation of the bubbling frequency as a function of the various pertinent parameters involved may be rewritten as follows (in the MKSA system):

$$f \approx 2.4 \times 10^{-14} \frac{\theta^2[c_L - k_H(P + 2\gamma/r)]}{\eta r(P + 2\gamma/r)\lambda \ln[(z_f + 10r)/(z_0 + 10r)]} \tag{19}$$

The boundary layer thickness λ was indirectly approached and found to be of the order of 20 µm (Liger-Belair *et al.*, 2005b). Finally, let us apply the latter equation to the standard textbook case fiber displayed in Fig. 1.8 and modeled in Fig. 1.11 (i.e., $r \approx 5$ µm, $z_0 \approx 20$ µm, and $z_f \approx 100$ µm). Eq. (19) may therefore be rewritten as follows, by replacing the fiber's parameters r, z_0, z_f, and λ by their numerical value:

$$f \approx 5.2 \times 10^{-8} \frac{\theta^2[c_L - k_H(P + 0.2)]}{\eta(P + 0.2)} \tag{20}$$

In the latter expression, f is expressed in bubbles/s, c_L is expressed in g/L, k_H in g/L/atm, P in atm, and η in kg/m/s, to fit the standards used in enology.

We will discuss the relative influence of the following parameters on the average bubbling frequency: (i) the concentration c_L of CO_2-dissolved molecules, (ii) the liquid temperature θ, and (iii) the ambient pressure P.

(i) Following Eq. (20), every other parameter being constant, the dependence of the theoretical average bubbling frequency f with the CO_2-dissolved concentration c_L is in the form $f = ac_L - b$. By use of a high-speed video camera fitted with a microscope objective, a few cellulose fibers acting as bubble nucleation sites on the wall of a glass poured with champagne were followed with time during the whole gas-discharging process (which may last up to several hours). This method is developed in minute details in Liger-Belair *et al.* (2001b). The dependence of the experimental bubbling frequency f_{exp} with c_L was found to follow a linear-like c_L dependence, as expected from the model developed above. Therefore, the frequency of bubble formation from a given nucleation site is found to progressively decrease with time, because the concentration c_L of CO_2-dissolved molecules progressively decreases as CO_2 continuously desorbs from the champagne matrix. Furthermore, it is worth noting that the bubbling frequency of a given nucleation site vanishes (i.e., the bubble release ceases, $f \to 0$ bubble/s), although the CO_2-dissolved concentration c_L remains higher than a critical value, as shown in Liger-Belair *et al.* (2001b). Actually, following both Laplace's and Henry's law, the curvature r of the CO_2 pocket trapped inside the fiber's lumen induces in the close vicinity of the trapped CO_2 pocket a concentration c_B of CO_2-dissolved molecules of order of $k_H(P_0 + 2\gamma/r)$. Consequently, as soon as the concentration of CO_2-dissolved in the liquid bulk reaches a critical value $c_L^* = c_B \approx k_H(P_0 + 2\gamma / r)$, the diffusion toward the gas pocket ceases and the given nucleation site stops releasing bubbles (simply because Δc, the driving force of diffusion, vanishes as $c_L \approx c_L^*$). Let us apply the latter condition to the characteristic radius of a cellulose fiber ($r \approx 5$ µm). At 10 °C, the critical concentration c_L^* below which bubble release becomes impossible is therefore:

$$c_L^* \approx k_H(P_0 + 2\gamma/r) \approx 2.07 \times 10^{-5}\left(10^5 + 2 \times 5 \times 10^{-2}/5 \times 10^{-6}\right) \approx 2.5\,\text{g/L} \tag{21}$$

(ii) The dependence of the bubbling frequency with the liquid temperature is much more difficult to test experimentally in real consuming conditions. Actually, we needed time to decrease or increase the liquid temperature, and we found no satisfying possibility of modifying the liquid temperature without significantly losing CO_2-dissolved molecules which continuously desorb from the supersaturated liquid matrix due to

diffusion through the liquid surface and due to bubbling from the numerous nucleation sites found in the flute. We will nevertheless discuss the theoretical influence of the liquid temperature by retrieving Eq. (20). In Eq. (20), the temperature directly appears as θ^2, but it is worth noting that the Henry's law constant k_H, as well as the champagne dynamic viscosity η, is strongly temperature dependent (Liger-Belair and Rochard, 2008). Therefore, increasing the liquid temperature by 10 K (let us say from 278 to 288 K, which is approximately the range of champagne-tasting temperatures) increases the theoretical bubbling frequency by about 50%. For the fiber displayed in Fig. 1.8 ($r \approx 5$ µm, $z_0 \approx 20$ µm, and $z_f \approx 100$ µm) and with $c_L \approx 12$ g/L, the theoretical temperature dependence of the bubbling frequency is displayed in Fig. 1.12.

(iii) Increasing or decreasing the ambient pressure P also significantly modifies the corresponding average bubbling frequency f. For the fiber displayed in Fig. 1.8 ($r \approx 5$ µm, $z_0 \approx 20$ µm, and $z_f \approx 100$ µm) and with $c_L \approx 12$ g/L, the theoretical pressure dependence of the bubbling frequency is displayed in Fig. 1.13. Reducing the ambient pressure to only 0.3 atm (e.g., on the top of Mount Everest) would increase the average bubbling frequency by a factor of almost 3. This is basically the same phenomenon which is responsible for gas embolism in divers who have

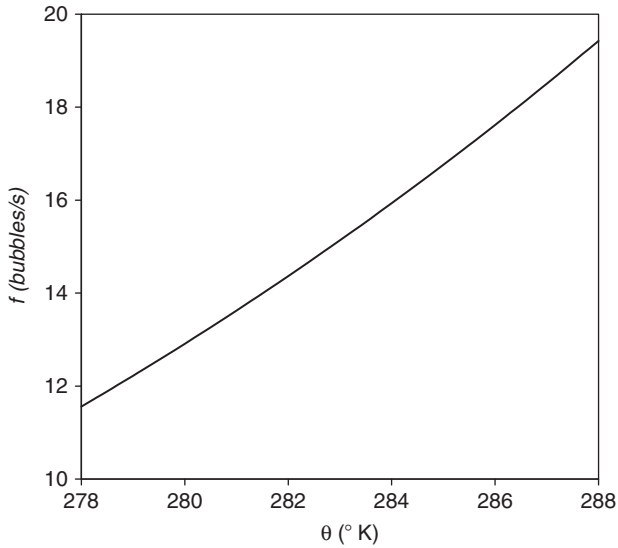

FIGURE 1.12 Theoretical dependence of the bubbling frequency f with the temperature θ, as expected from the model displayed in Eq. (20), in the range of usual champagne-tasting temperatures (from 5 to 15 °C), and for the textbook case fiber displayed in Fig. 1.7.

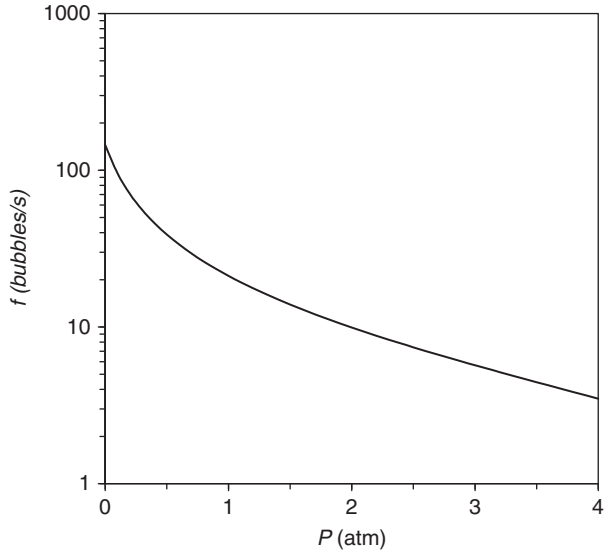

FIGURE 1.13 Theoretical dependence of the bubbling frequency f with the ambient pressure P (at 20 °C), as expected from the model displayed in Eq. (20) for the textbook case fiber displayed in Fig. 1.7.

breathed high-pressure air under water if they resurface too quickly. Inversely, increasing the ambient pressure to 2 atm decreases the average bubbling frequency by a factor of about 2 compared to that at sea level.

E. Evidence for bubbling instabilities

The regular and clockwork release of bubbles from a cellulose fiber is indeed the most common and usual way of forming bubbles, but cellulose fibers were recently found to experience other various and sometimes very complex rhythmical bubbling regimes (Liger-Belair *et al.*, 2005a, 2006b). After pouring champagne into a flute, a thorough examination (even by the naked eye) of the bubble trains rising toward the liquid surface recently revealed a curious and quite unexpected phenomenon. As time proceeds, during the gas-discharging process from the liquid matrix, some of the bubble trains showed abrupt transitions during the repetitive and rhythmical production of bubbles. Visually speaking, the macroscopic pertinent parameter which is characteristic from the successive bubbling regimes is the interbubble distance between the successive bubbles of a given bubble train. In Fig. 1.14, micrographs of a bubble train in its successive rhythmical bubbling regimes while degassing are displayed. The duration of a given bubbling regime may vary from a few

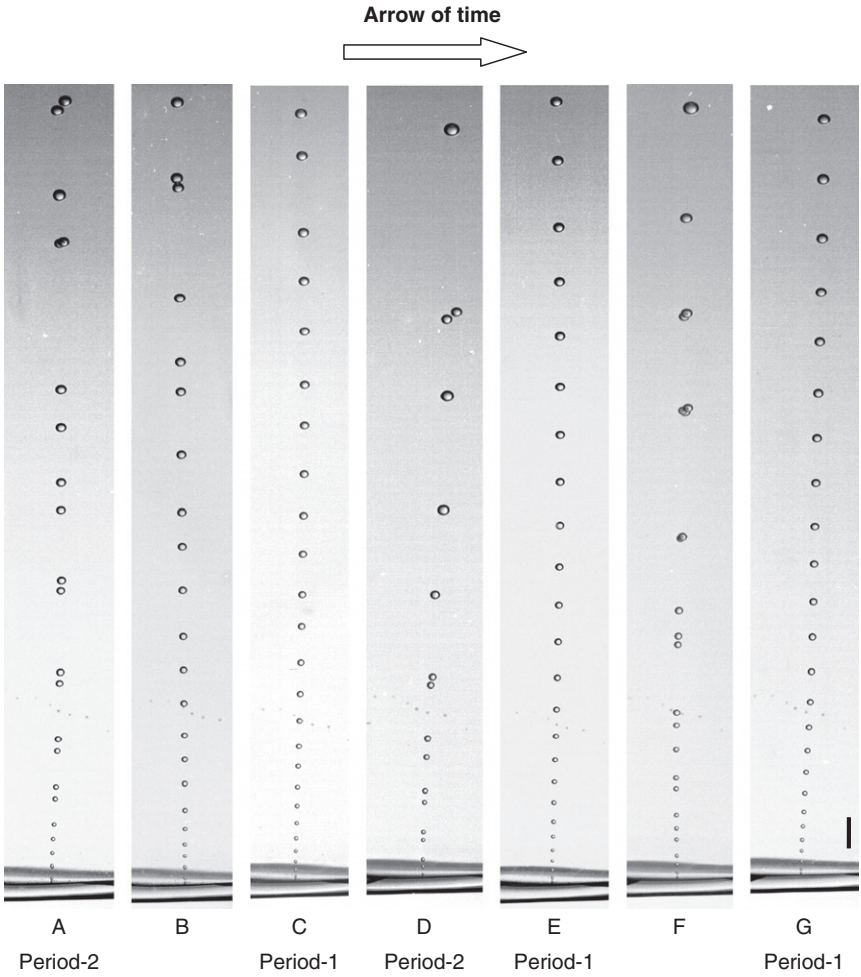

FIGURE 1.14 Time sequence (from left to right) showing a bubble nucleation site at the bottom of a flute poured with champagne blowing bubbles through different and well-established bubbling regimes (bar = 1 mm; photographs by Gérard Liger-Belair).

seconds to several minutes. In frame (a), bubbles are seen to be generated from a period-2 bubbling regime which is characterized by the fact that two successive bubbles rise by pairs. Then, the bubbling regime suddenly changes, and a multiperiodic bubbling regime arises which is displayed in frame (b). Later, in frame (c), clockwork bubbling in period-1 occurs where the distance between two successive bubbles increases monotonically as they rise, and so on. This nucleation site experienced other various bubbling regimes during its life, until it finally ended in a clockwork period-1 bubbling regime presented in frame (g).

Such a curious and unexpected observation raises the following question: what is/are the mechanism(s) responsible for the transitions between the different bubbling regimes? To better identify the fine mechanisms behind this rhythmical production of bubbles from a few nucleation sites, some of them experiencing bubbling transitions were filmed *in situ* by use of a high-speed digital video camera. Two time sequences are displayed in Figs. 1.15 and 1.16, where bubbles are blown in a period-2 and in a very erratic way, respectively. The lumen of the cellulose fiber displayed in Fig. 1.15 presents only one gas pocket, whereas the fiber's lumen displayed in Fig. 1.16 clearly shows two gas pockets periodically touching and connecting themselves through a tiny gas bridge (see frames 3 and 4 of Fig. 1.16). The micrometric gas bridge connecting the two gas pockets and disturbing the overall production of bubbles is enlarged in Fig. 1.17. This tiny gas bridge is a likely source of bubbling instabilities. Recently, a model was built which takes into account the coupling between the bubbling frequency and the frequency of the single gas pocket which oscillates while trapped inside the fiber's lumen (e.g., as in Fig. 1.15). The previously published data showed a general rule concerning bubbling instabilities arising from some fibers presenting just one trapped gas pocket. In this previous paper, the successive rhythmical bubbling regimes followed the so-called ''period-adding scenario'' (Liger-Belair *et al.*, 2005a).

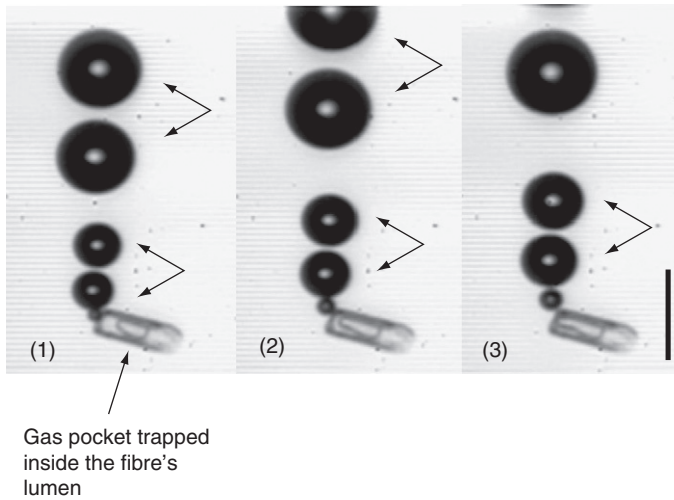

FIGURE 1.15 Close-up time sequence illustrating a tiny cellulose fiber acting as a bubble nucleation site in its period-2 bubbling regime (i.e., bubbles are blown by pairs); the time interval between two successive frames is 40 ms (bar = 50 μm; photographs by Gérard Liger-Belair).

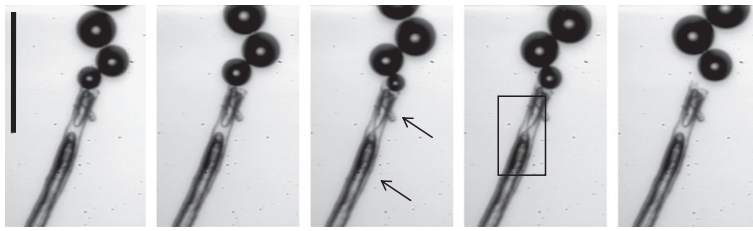

FIGURE 1.16 Two gas pockets are interacting in the lumen of this cellulose fiber, thus disturbing the periodicity of the bubbling regime; the black arrows point the various gas pockets interacting; the time interval between two successive frames is 10 ms (bar = 100 μm; photographs by Gérard Liger-Belair).

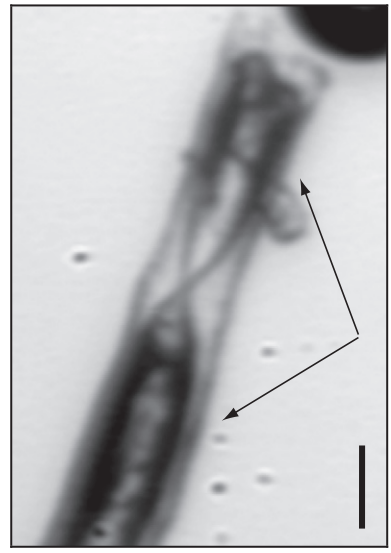

FIGURE 1.17 Detail of the cellulose fiber displayed in Fig. 1.16, which clearly shows the establishment of a micrometric gas bridge between the two gas pockets trapped inside the fiber's lumen (bar = 10 μm; photograph by Gérard Liger-Belair).

Nevertheless, this previously published scenario does not fit the various ways of forming bubbles from more complex cellulose fibers able to entrap numerous gas pockets, as shown in Fig. 1.16. Numerous fibers, such as those shown in the present paper, presented a sequence of various bubbling instabilities which is not reproduced by our previous model. A huge collection of successive rhythmical bubbling regimes has already been observed, and the highest recorded periodicity was observed for a fiber presenting a period-12 bubbling regime (Liger-Belair *et al.*, 2006b). At the moment, we could not find any general rule

with fibers presenting numerous gas pockets interacting together, but the close-up observation and the discovery of the multiple gas pockets interacting together are considered as a step toward a deeper understanding of the successive rhythmical bubbling regimes arising from complex fibers. The huge diversity of our observations, in terms of the various successive bubbling regimes seems to be directly linked with the ''natural'' variability of cellulose fibers (in terms of size, lumen diameter, inner wall properties, etc.).

F. "Artificial" bubble nucleation

Artificial effervescence is related to bubbles nucleated from glasses imperfections done intentionally by the glassmaker to promote or to eventually replace a deficit of ''natural'' nucleation sites. Actually, it has been known for decades that bubbles may arise from microscratches on the glass wall (Lynch and Bamforth, 2002; Ronteltap *et al*., 1991) Those microscratches are geometrically able to trap tiny air pockets when champagne is poured into the glass (as cellulose fibers do). Those microscratches on a glass can be done by essentially two techniques: sandblast or laser engraving. Nevertheless, effervescence produced from scratches intentionally done by the glassmaker does not resemble that arising from tiny individual cellulose fibers. A rendering of such microscratches releasing bubbles at the bottom of a champagne flute is displayed in Fig. 1.18. It is worth noting that the repetitive bubbling process arising from artificial bubble nucleation is much more vigorous and chaotic than the bubbling process from tiny cellulose fibers. Glasses engraved at their bottom are thus indeed easily recognizable, with a characteristic bubble column rising on their axis of symmetry (Liger-Belair *et al*., 2007; Polidori *et al*., 2008). Effervescence promoted by engraved glasses is indeed visually quite different than that naturally promoted by cellulose fibers, but the difference is also suspected to go far beyond the solely esthetical (and rather subjective) point of view. Differences are strongly suspected concerning the kinetics of CO_2 and flavor release all along champagne tasting.

IV. DURING THE BUBBLE RISE

A. Bubble growth

After being born on micrometric gas pockets trapped inside impurities of the glass wall, bubbles rise toward the liquid surface due to their own buoyancy. While rising, they continue to grow in size by continuously absorbing carbon dioxide molecules dissolved into the liquid ''matrix'', as

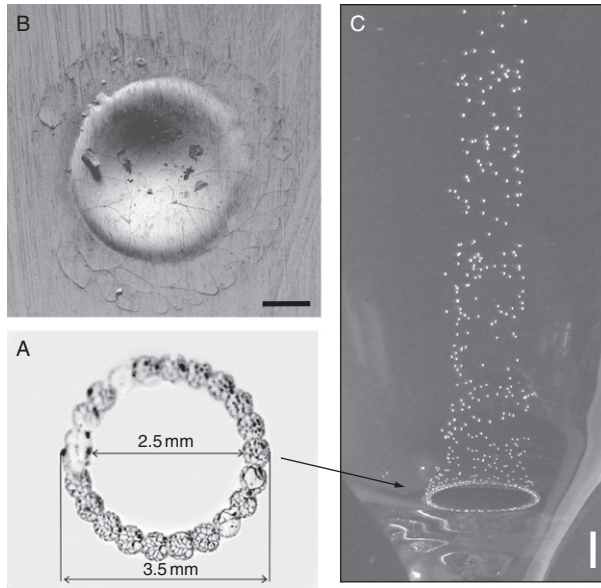

FIGURE 1.18 At the bottom of this flute, on its axis of symmetry, the glassmaker has engraved a small ring (done with adjoining laser beam impacts) (A); single laser beam impact as viewed through a scanning electron microscope (bar = 100 μm) (B); effervescence in this flute is promoted from these "artificial" microscratches into the form of a characteristic and easy recognizable vertical bubbles column rising on its axis of symmetry (bar = 1 mm; photographs by G. Polidori and F. Beaumont) (C).

it is clearly illustrated on the photograph displayed in Fig. 1.19. Growing bubbles thus continuously accelerate along their way through the champagne. This continuous acceleration is also betrayed, on high-speed photographs, by the continuously increasing spacing e between the successive bubbles of a given bubble train, as seen in Fig. 1.19, for example.

High-speed photography and strobe lighting were used to monitor the motion of bubbles (Liger-Belair, 2002). It was found that the bubble radius R of bubbles increases at a constant rate $k = \mathrm{d}R/\mathrm{d}t$, as they rise toward the liquid surface. Thus,

$$R(t) = R_0 + kt \tag{22}$$

where R_0 is the bubble radius as it detaches from the nucleation site. R_0 is of the same order of magnitude than the radius of the mouth of the cellulose fiber which acts as a nucleation site, that is, around 5–10 μm (Liger-Belair, 2002; Liger-Belair *et al.*, 2005b).

The first experimental observations about the growth and rise of bubbles in carbonated beverages were conducted in the early 1990s, with bubbles rising and growing in a glass of beer (Shafer and Zare,

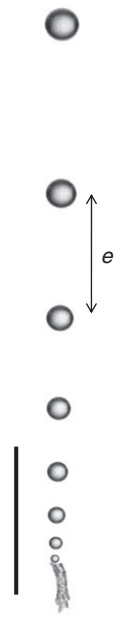

FIGURE 1.19 A characteristic bubble train promoted by the repetitive bubble formation processes from a single cellulose fiber; bubbles are clearly seen growing during their way up (bar = 1 mm; photograph by Gérard Liger-Belair).

1991). Shafer and Zare also proved that bubbles' diameter linearly increases with time as bubbles rise toward the liquid surface.

Three minutes after pouring, experiments conducted with Champagne and other sparkling wines led to growth rates k ranging between 350 and 400 μm/s, at 20 °C. (Liger-Belair, 2002). Experiments were also performed with bubbles rising in beer glasses. In beer, 3 min after pouring, bubble growth rates were found to lay around 100–150 μm/s, that is, about three times less than those in Champagne and other sparkling wines (Liger-Belair, 2002). By use of mass transfer equations, the growth rate k of bubbles rising in champagne and beer (at low to moderate Reynolds numbers) was also modeled and linked with some physicochemical properties of liquids as follows (in the MKSA system):

$$k = \frac{\mathrm{d}R}{\mathrm{d}t} \approx 0.63 \frac{\Re\theta}{P_{\mathrm{B}}} D_0^{2/3} \left(\frac{2\alpha\rho g}{9\eta}\right)^{1/3} \Delta c \tag{23}$$

where θ is the liquid temperature, $\Re$ the ideal gas constant, P_{B} the pressure inside the rising bubble, D_0 the diffusion coefficient of CO_2 molecules through the liquid bulk, ρ and η are, respectively, the liquid density and viscosity, g the acceleration due to gravity, α a numerical

prefactor close to 0.7 for Champagne and other sparkling wines bubbles, h the distance traveled by the bubble from its nucleation site, and Δc (the driving force responsible for the diffusion of CO_2 into the rising bubble) is the difference in dissolved-CO_2 concentrations between the liquid bulk and the close vicinity of the bubble surface in equilibrium with the gaseous CO_2 into the rising bubble (see Fig. 1.20).

Strictly speaking, the pressure P_B inside the rising bubble is the sum of three terms: (i) the atmospheric pressure P_0, (ii) the hydrostatic pressure ρgH, and (iii) the Laplace pressure $2\gamma/R$, originated in the bubble's curvature. H is the depth at which the bubble rises and γ is the surface tension of the liquid medium. However, H varying from several millimeters to several centimeters, the surface tension of champagne being of the order of 50 mN m^{-1}, and bubbles' radii varying from several tens to several

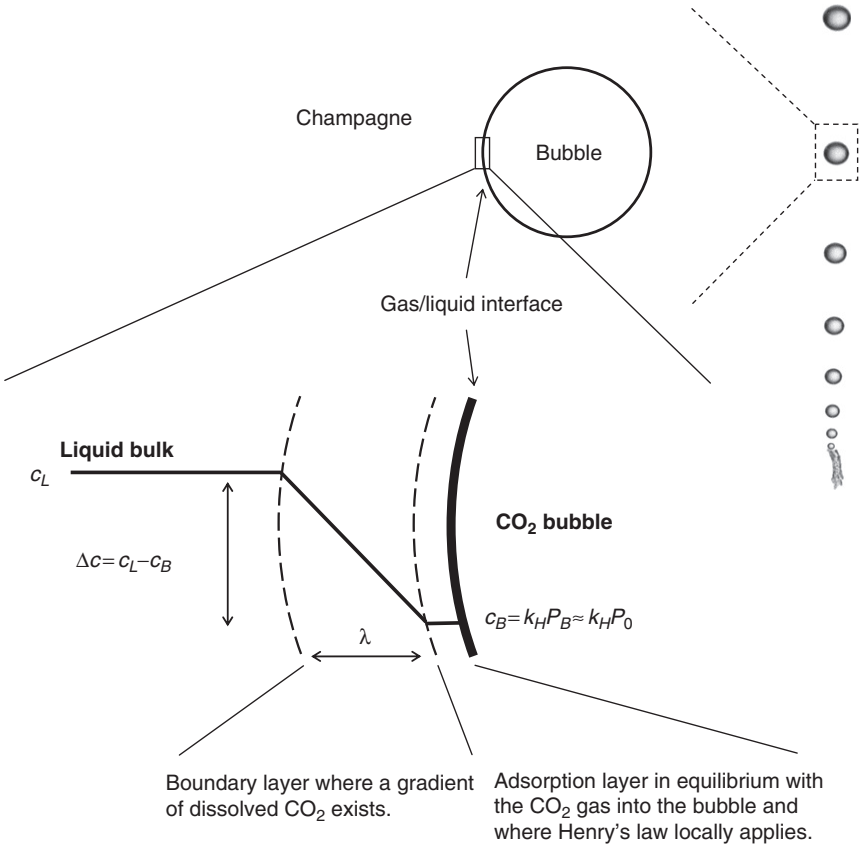

FIGURE 1.20 Carbon dioxide concentrations in the close vicinity of the CO_2 bubble surface.

hundreds of micrometers, the contribution of both hydrostatic and Laplace pressures is clearly negligible in front of the atmospheric pressure P_0.

Let us test the applicability of Eq. (23) in case of rising and expanding champagne bubbles, at 20 °C. By using known values of ρ and η in champagne (Liger-Belair, 2002) $\alpha = 0.7$, $D_0 \approx 1.4 \times 10^{-9}$ m^2/s, as measured by Nuclear Magnetic Resonance (Liger-Belair *et al.*, 2003), and the difference in CO_2 concentrations between the liquid bulk and the close vicinity of the bubble surface $\Delta c \approx 10$ g/L ≈ 227 mol/m^3, one finds

$$k \approx 0.63 \times \frac{8.31 \times 293}{10^5} \times \left(1.4 \times 10^{-9}\right)^{2/3} \times \left[\frac{2 \times 0.7 \times 10^3 \times 9.8}{9 \times 1.5 \times 10^{-3}}\right]^{1/3} \times 227 \approx 500\,\mu\text{m/s} \tag{24}$$

which is in quite good accordance with the order of magnitude of experimentally observed growth rates (Liger-Belair, 2002). This value nevertheless slightly overestimates experimentally observed growth rates probably because, 3 min after pouring, champagne already lost a significant part of its dissolved-CO_2 content, thus decreasing Δc below its initial value of 227 mol/m^3.

Very recently also, Zhang and Xu proposed a model for the growth rate of rising bubbles in both champagne and beer (Zhang and Xu, 2008).

B. Average bubble size

Because champagne and other sparkling wine tasters are often concerned with the size of bubbles formed in the wine (a proverb says that the smaller the bubbles, the better the wine), much attention was paid recently to model the average size of ascending bubbles. Actually, the final average size of ascending bubbles is the result of a combination between their growth rate and their ascending velocity. Recent calculations, based on mass transfer equations, linked the final average bubbles' size with various physicochemical and geometrical parameters (Liger-Belair, 2005, 2006). The following dependence of the ascending bubble radius R with some of the liquid parameters was derived (in the MKSA system):

$$R \approx 1.24 \left(\frac{9\eta}{2\alpha\rho g}\right)^{2/9} \left(\frac{\Re\theta}{P_B}\right)^{1/3} {D_0}^{2/9} (\Delta c)^{1/3} h^{1/3} \tag{25}$$

To go further on with the dependence of bubbles' radii with some few parameters, we can also replace in the latter equation the diffusion coefficient D_0 by its theoretical expression approached through the well-known Stokes–Einstein equation ($D_0 \approx k_B\theta / 6\pi\eta d$). The following relationship expressed in the MKSA system was thus obtained:

$$R(h,\theta,\ldots) \approx 2.5\left(\frac{3k_B}{4\pi\alpha r}\right)^{2/9}\left(\frac{1}{\rho g}\right)^{2/9}\left(\frac{1}{P_0}\right)^{1/3}\theta^{5/9}(c_L - c_B)^{1/3}h^{1/3} \quad (26)$$

It is worth noting that the dependence of the bubble size with the liquid viscosity vanishes. Finally, by replacing in Eq. (26), k_B, α, and d by their known numerical values, and by developing c_B as $k_H P_0$, one obtains

$$R \approx 2.7 \times 10^{-3}\theta^{5/9}\left(\frac{1}{\rho g}\right)^{2/9}\left(\frac{c_L - k_H P_0}{P_0}\right)^{1/3}h^{1/3} \quad (27)$$

Otherwise, because the liquid density ρ does not significantly vary from one champagne to another (and even from one carbonated beverage to another), we will discuss and put the accent on the influence of the following parameters on the bubble size: (i) the traveled distance h, (ii) the liquid temperature θ, (iii) the gravity acceleration g, (iv) the ambient pressure P_0, and (v) the carbon dioxide content c_L.

(i) The longer the traveled distance h, the larger the bubble size. This dependence of the bubble size with its traveled distance through the liquid means that, during champagne tasting, the average bubble size at the champagne surface varies from one glass to another. In a narrow flute, for example, the level of champagne poured is about three times higher than that in a typical coupe (with a shallower bowl and a much wider aperture). Therefore, the average bubbles' diameters in the flute will be larger than those in the coupe by a factor of about $R_{flute} / R_{coupe} \approx 3^{1/3} \approx 1.45$ (i.e., bubbles about three times larger in volume), as seen in the photograph displayed in Fig. 1.21, which compares the average size of bubbles after pouring, whether champagne is served into a flute or into a coupe.

(ii) In Eq. (27), the temperature appears directly as $\theta^{5/9}$, but we should not forget that the Henry's law constant k_H is also strongly temperature dependent (see Fig. 1.2) and conveniently expressed by the Van't Hoff Eq. (3). The temperature being expressed in K, the temperature dependence of the bubble size is nevertheless quite weak. Increasing the liquid temperature by 10 K (let us say from 278 to 288 K, which is approximately the range of champagne-tasting temperature) makes bubbles grow from about only 5–6% in diameter.

(iii) The gravity acceleration which is the driving force behind the bubble rise (through buoyancy) also plays quite an important role in the final bubble's size. This could indeed be easily evidenced during a parabolic flight where the acceleration changes from microgravity (close to zero-g) to macrogravity (up to $1.8 \times g$). On the Moon, for example, where the gravity is about one-sixth the gravity on Earth, the average

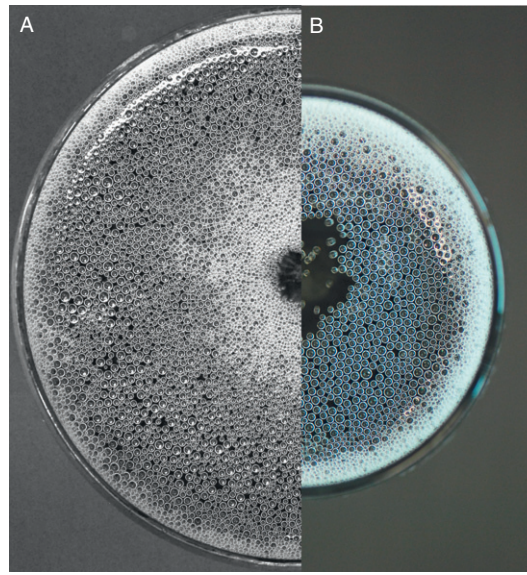

FIGURE 1.21 Bubbles' size distribution at the free surface of champagne, 30 s after pouring, whether champagne is served in the coupe (A) or in the flute (B) engraved on its bottom. Because of the drastic glass washing protocol, bubbles were generated only from nucleation sites of the ring-shaped engravements (lying respectively, 2.9 and 7.4 cm below the free surface area, whether champagne is served in the coupe or in the flute; photographs by Gérard Liger-Belair).

bubbles' size would increase by a factor of about $g_{\text{Moon}} / g_{\text{Earth}} \approx 6^{2/9} \approx 1.49$ (i.e., bubbles almost 50% larger in diameter and therefore more than three times larger in volume).

(iv) The pressure inside the rising bubble is equivalent to the ambient pressure P_0 (for the reasons detailed in the latter paragraph). Usually, at the sea level, this pressure is equivalent to 1 atm (or 10^5 N/m). Reducing the atmospheric pressure to only 0.3 atm (on the top of Mount Everest, e.g.) would increase the average bubble diameter by about 55% (and therefore by a factor of almost 4 in volume).

(v) The carbon dioxide content of the liquid medium c_L also influences the final average bubbles' size. This is the main reason why bubbles in beer are significantly smaller than bubbles in champagne and other sparkling wines. Actually, the carbon dioxide content in beers may classically vary from about 4 to 7 g/L, whereas the carbon dioxide content in champagne and other sparkling wines may rather vary from 10 up to 12 g/L (i.e., c_L is approximately two times higher in champagne than in beer). Reducing c_L by a factor 2 in Eq. (27) would decrease the theoretical average bubble size by about 40% (thus leading to bubbles almost five times smaller in volume). The two

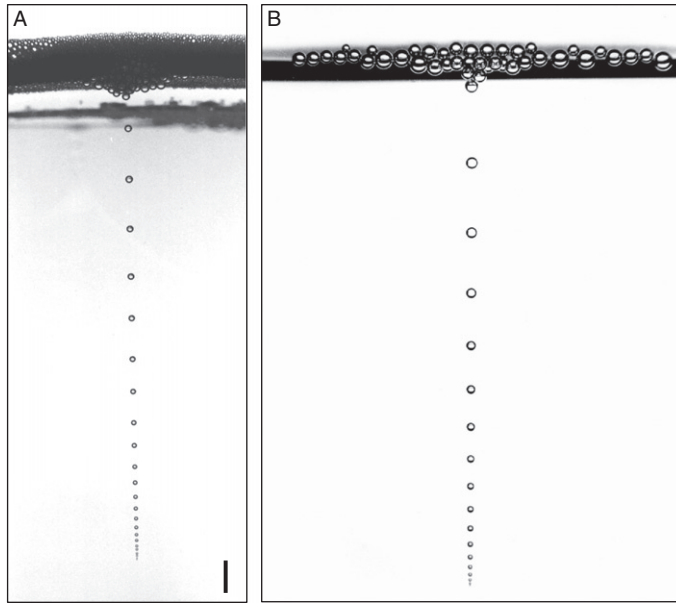

FIGURE 1.22 Three minutes after pouring, bubbles rising in a glass of beer (A) show diameters much lower than those of bubbles rising in a flute poured with champagne (B) (bar = 1 mm); the very significant difference between the bubble size in champagne and beer is mainly due to amounts of dissolved-CO_2 about two times higher in champagne than in beer (photographs by Gérard Liger-Belair).

photographs displayed in Fig. 1.22 illustrate the significant difference in bubble size between a standard commercial champagne and a standard commercial beer, both showing very typical bubbling behavior. Moreover, after pouring champagne into a flute, due to bubbling and diffusion through the surface of champagne, CO_2 molecules progressively escape from the liquid medium. Subsequently, the dissolved carbon dioxide content c_L in the liquid medium progressively decreases. Therefore, as time proceeds during champagne tasting, the average bubbles' size at the liquid surface progressively decreases, as can be clearly seen in the sequence displayed in Fig. 1.23.

V. CO_2 VOLUME FLUXES OUTGASSING FROM CHAMPAGNE GLASSES IN TASTING CONDITIONS

A. Flute versus coupe

In case of champagne and other sparkling wine tasting, two quite emblematic types of drinking vessels have coexisted for decades: (i) the classical flute, namely, a long-stemmed glass with a deep tapered bowl

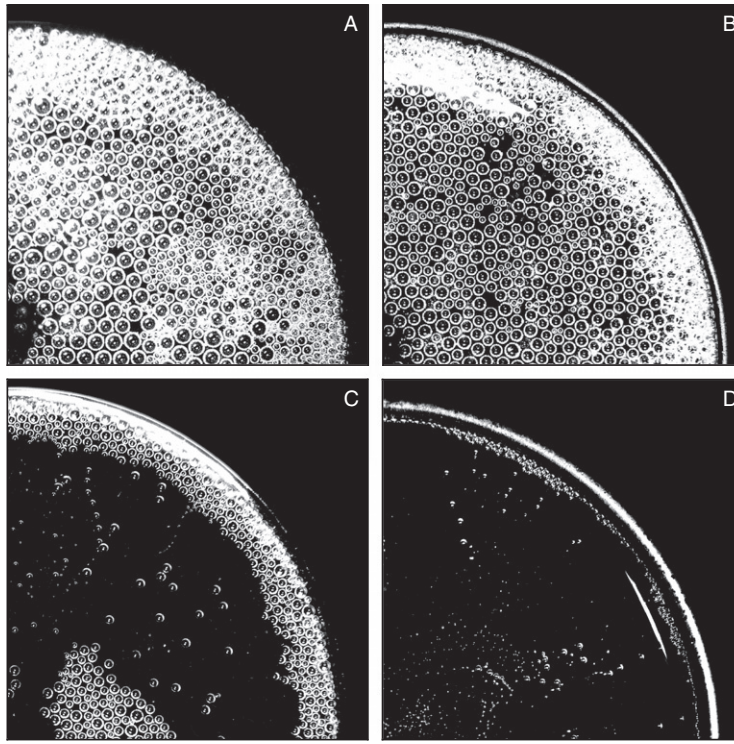

FIGURE 1.23 Time sequence showing successive top views of a flute poured with champagne and followed as time proceeds; (A) immediately after pouring, (B) 3 min after pouring, (C) 10 min after pouring, and (D) 25 min after pouring; it clearly appears that the average bubbles' size decreases as time proceeds, as well as the average number of floating bubbles (photographs by Gérard Liger-Belair).

and a narrow aperture, and (ii) the classical coupe, namely, a shallower glass with a much wider aperture. Advantages and disadvantages of both glass shapes have long been debated, nevertheless without bringing any sensory and/or analytical data. Due to their very different geometrical properties, the kinetics of CO_2 release has therefore been supposed to significantly differ between these two different kinds of champagne-drinking vessels. Very recently, measurements of CO_2 volume fluxes outgassing from champagne were done, during the first 10 min following pouring (Liger-Belair *et al.*, 2009c). In order to avoid the randomly located ''bubbling environment'' inevitably provided in glasses showing natural effervescence, single standard flutes and coupes engraved on their bottoms were used for this set of experiments (thus providing a ''standardized'' and artificial effervescence, as that displayed in Fig. 1.18). Between the successive pouring and time series data recordings, the flute and the

coupe were systematically and thoroughly washed in a dilute aqueous formic acid solution, rinsed using distilled water, and then compressed air dried. This drastic treatment limits the potential formation of calcium carbonate crystals on the flute wall as well as the adsorption of any dust particle acting as ''natural'' bubble nucleation sites. With such a surface treatment, CO_2 bubble nucleation is strictly restricted to the bubble nucleation sites of the ring-shaped engravement, so that differences in the kinetics of CO_2 release from one type of drinking vessel to another are attributed only to geometrical differences between them (assuming identical etching).

1. Evidence for losses of dissolved CO_2 during champagne serving

The pouring process is far from being consequence-less with regard to the dissolved CO_2 concentration c_L (Liger-Belair *et al.*, 2009b,c). During the several seconds of the pouring process inevitably preceding tasting, champagne undergoes highly turbulent and swirling flows. During this phase, champagne loses quite a significant part of its initial content in dissolved CO_2. Consequently, as soon as champagne is served and ready to drink, CO_2 dissolved in champagne is suspected to be well below its initial content of about 11.5 g/L (as chemically measured inside a bottle, after uncorking, but before pouring). The initial bulk concentration of dissolved CO_2 after pouring, denoted c_i, was chemically accessed by using carbonic anhydrase. The official method used to measure the dissolved CO_2 content is thoroughly detailed in two recent papers (Autret *et al.*, 2005; Liger-Belair *et al.*, 2009b). To enable a statistical treatment, six successive CO_2-dissolved measurements were systematically done for each type of drinking vessel, after six successive pouring (from six distinct bottles). Champagne was found to initially hold (after pouring) a concentration of CO_2-dissolved molecules of $c_i^{flute} = 7.4 \pm 0.4$ g/L in the flute, and $c_i^{coupe} = 7.4 \pm 0.5$ g/L in the coupe (i.e., approximately 4 g/L less in both types of drinking vessels after pouring than inside the bottle, before pouring).

Table 1.3 summarizes the geometrical and analytical pertinent parameters linked with each type of drinking vessel poured with 100 mL of champagne. Turbulences of the pouring process therefore cause

TABLE 1.3 Pertinent parameters linked with each type of drinking vessel filled with 100 mL of champagne

Type of vessel	Liquid level after pouring, h (cm)	Surface area offered to gas discharge, A (cm)	Initial concentration of dissolved CO_2, c_i (g/L)
Flute	7.4	21.2	7.4 ± 0.4
Coupe	2.9	60.8	7.4 ± 0.5

significant and quite unexpected loss of dissolved CO_2 during champagne serving. It is worth noting that losses of CO_2-dissolved molecules during the pouring process are of the same order of magnitude whether champagne is served in the flute or in the coupe, despite a significantly longer pouring process in the case of the flute (mainly due to an excess of foam restricted in narrower aperture, which forces the taster to pour champagne into the flute in two or three steps in order to avoid champagne overflow). This observation first appeared counter intuitive to us. Actually, losses of dissolved CO_2 induced by a longer pouring process in the flute could be counterbalanced by the much larger area offered to CO_2-dissolved molecules escape in case of the coupe aperture.

2. Influence of each type of drinking vessel on its loss of dissolved CO_2 concentration with time

For each type of drinking vessel, the corresponding loss of dissolved CO_2 concentration with time along the first 10 min following pouring is displayed in Fig. 1.24.

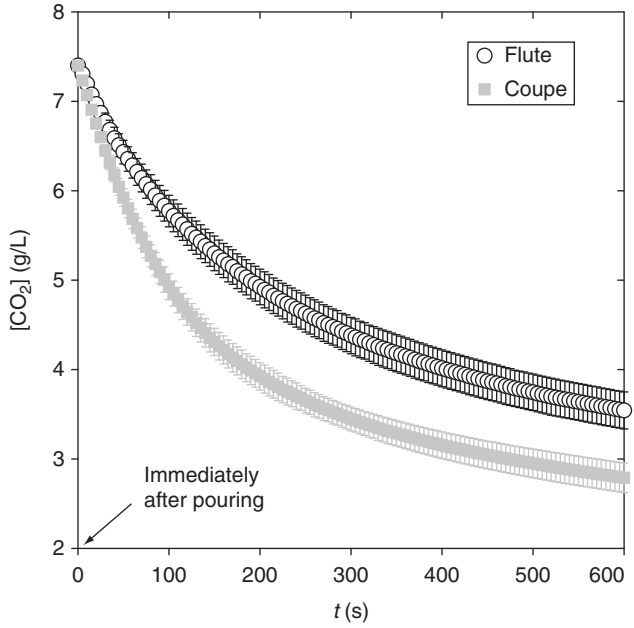

FIGURE 1.24 Progressive loss of CO_2-dissolved concentrations (in g L^{-1}) all along the first 10 min following the pouring process in a flute and in a coupe, respectively, filled with 100 mL of champagne; each datum of each time series is the arithmetic average of six successive values recorded from six successive pouring; standard deviations correspond to the root-mean-square deviations of the values provided by the six successive data recordings.

Despite significant standard deviations (mainly attributed to the difficult repeatability of the manual pouring process between the six successive pouring and time series data records conducted for each type of drinking vessel), it is clear from Fig. 1.24 that the progressive loss of dissolved CO_2 concentration with time is significantly higher when champagne is served in the coupe than in the flute. From the taster point of view, this observation is of importance for both the visual aspect of champagne and its ''mouth feel'' sensation. Actually, it was recently shown that the higher the concentration of dissolved CO_2 in champagne, the higher the kinetics of bubble nucleation, the larger the average bubbles' size, and finally the more effervescence in the glass (Liger-Belair, 2005). Moreover, it is also well known in champagne and other sparkling wine tasting that the higher the concentration of dissolved CO_2, the higher the ''fizzy'' sensation when bubbles burst over the tongue (Liger-Belair, 2009; Liger-Belair and Rochard, 2008). To the best of our knowledge, this is the first set of analytical results concerning the influence of glass shape on its progressive loss of dissolved CO_2 concentrations with time in tasting conditions, and therefore the first analytical proof that a long-stemmed glass with a deep tapered bowl and a narrow aperture prolongs the drink's chill and helps to retain its effervescence by contrast with a shallower coupe of much wider aperture.

3. Influence of each type of drinking vessel on CO_2 volume fluxes outgassing from it

In champagne and other sparkling wine tasting, in addition to the visual aspect of effervescence and mouth feel—both depending (among many other parameters) on the dissolved-CO_2 concentration $c(t)$—an other important aspect is the smell or ''nose'' of the wine, the so-called ''bouquet'' (Priser *et al.*, 1997; Tominaga *et al.*, 2003). Effervescence of champagne and other sparkling wines is suspected to promote the development of aromas in the headspace above the glass. The myriad of bubbles nucleating on the flute's wall and traveling through the wine's bulk is expected to enhance the release of volatile organic compounds by considerably enhancing exchange surfaces between the wine and the atmosphere. It is worth noting that, in a typical flute poured with champagne or sparkling wine, approximately 50,000 bubbles would have already nucleated, rose, and finally exploded during the first 3 min following pouring (Liger-Belair, 2002). Each bubble having a diameter close to 1 mm, this cloud of 50,000 bubbles totalizes a global exchange surface of approximately 1500 cm^2 during the first 3 min following pouring. This is huge compared with the area of the air–wine interface which rarely exceeds 20 cm^2 in a classical flute. However, each bubble collapsing at the wine's surface inevitably frees its tiny CO_2 volume. Consequently, the inevitable counterparty of the ''exhausting'' aromas effect attributed to

bubbles' exchange surfaces is to progressively bring gaseous CO_2 in the headspace above the wine's surface. It is indeed well known that a sudden and abundant quantity of CO_2 may irritate the nose during the evaluation of aromas (Liger-Belair and Rochard, 2008).

The analytical parameter which characterizes the progressive release of gaseous CO_2 desorbed from a glass poured with champagne is the total volume flux of CO_2 escaping from the wine–air interface. The total CO_2 volume fluxes outgassing from each type of drinking vessel poured with 100 mL of champagne are presented in the graph displayed in Fig. 1.25, during the first 10 min following the pouring process. Experimentally, during approximately the first 3 min following the pouring process, it is clear that total CO_2 volume fluxes are significantly higher when champagne is served in the coupe than in the flute. Nevertheless, this tendency reverses from about 3 min until 10 min after pouring, and total CO_2 volume fluxes outgassing from the flute become higher than those outgassing from the coupe (see the inset in Fig. 1.25).

In a recent paper, it was demonstrated that the driving force behind the progressive desorption of CO_2 from a glass poured with champagne

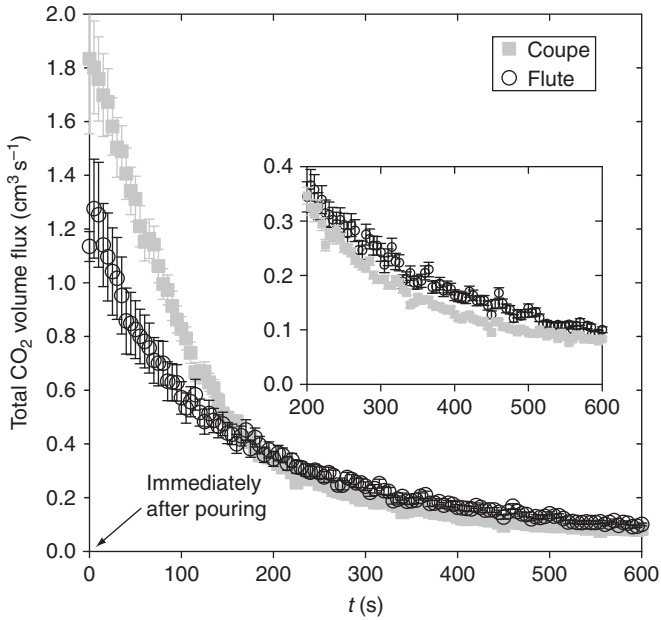

FIGURE 1.25 Total CO_2 volume fluxes recordings (in $cm^3\ s^{-1}$) desorbing from a flute and coupe, respectively, filled with 100 mL of champagne, all along the first 10 min following the pouring process; each datum of each time series is the arithmetic average of six successive values recorded from six successive pourings.

was its bulk concentration c_L of dissolved CO_2 (Liger-Belair *et al.*, 2009b). Therefore, it seemed pertinent to propose a correlation between the CO_2 volume flux outgassing from the flute and the continuously decreasing bulk concentration c_L of dissolved CO_2. To do so, time series data recordings displayed in Figs. 1.24 and 1.25 were combined. Time was eliminated so that the total CO_2 volume flux outgassing from each type of drinking vessel was plotted as a function of champagne dissolved CO_2 concentration c_L. Correlations between total CO_2 volume fluxes and dissolved CO_2 concentrations in champagne are displayed in Fig. 1.26, for each type of drinking vessel.

It is clear from Fig. 1.26 that, for a given dissolved CO_2 concentration of champagne, total CO_2 volume fluxes are significantly higher when champagne is served into a coupe than when it is served into a flute. Nevertheless, it is worth noting that from the point of view of champagne and other sparkling wine tasting, the pertinent parameter which characterizes a given type of drinking vessel with regard to its progressive CO_2 release with time is not really the total CO_2 volume flux outgassing from it. Actually, the open aperture of tasters' nostrils being obviously much

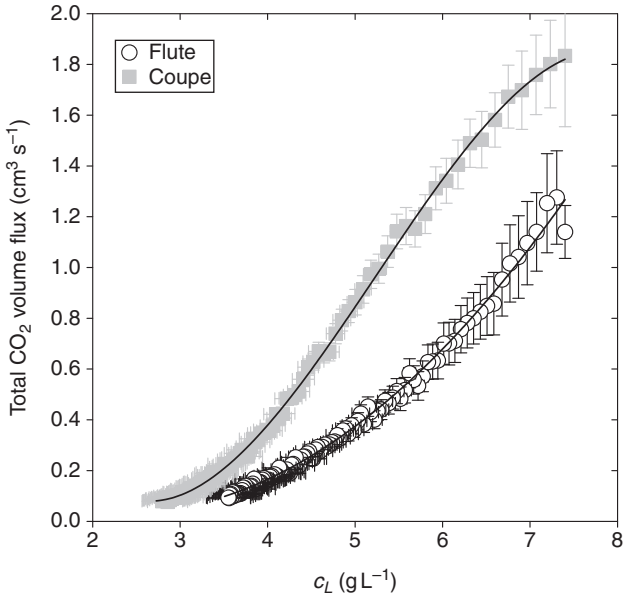

FIGURE 1.26 Total CO_2 volume fluxes recordings (in $cm^3\ s^{-1}$) desorbing from a flute and coupe, respectively, filled with 100 mL of champagne as a function of their dissolved-CO_2 concentration; each data of each time series is the arithmetic average of six successive values recorded from six successive pourings; experimental data were fitted with polynomial functions which appear as dashed lines.

smaller than the surface area of the drinking vessel offered to total gas discharge, we propose a more adapted analytical parameter in order to compare the progressive CO_2 release from various glasses, namely, the CO_2 volume flux per unit surface area, denoted F_{US}, and deduced as follows for each type of drinking vessel:

$$F_{US} = \frac{F_T}{A} \tag{28}$$

with A being the free surface area of the given type of drinking vessel (given in Table 1.3). CO_2 volume fluxes per unit surface area outgassing from each type of drinking vessel poured with 100 mL of champagne are presented in Fig. 1.27, during the first 10 min following the pouring process. It is clear from Fig. 1.27 that CO_2 volume fluxes outgassing per unit surface area are much higher in the flute than in the coupe, during the 10 min following the pouring process. From the point of view of champagne tasting, it means that the flute should finally enable higher concentrations of gaseous CO_2 above the champagne free surface during tasting (due to its narrower open aperture compared to that of the coupe), despite lower total CO_2 volume fluxes in the first 3 min following pouring. Further determination of the gaseous CO_2 concentration above

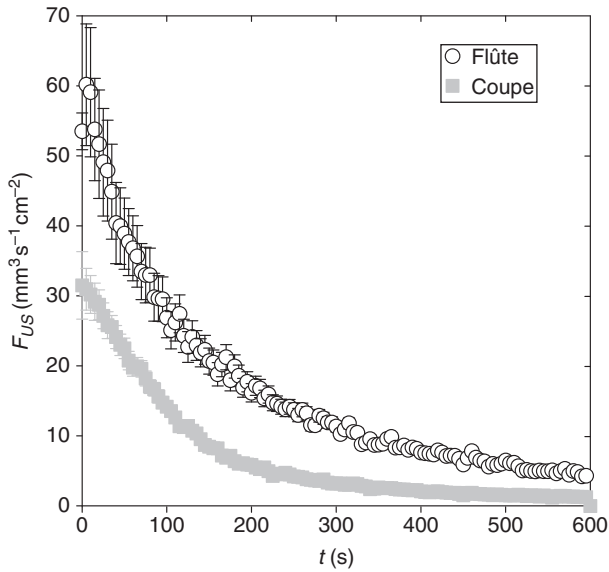

FIGURE 1.27 CO_2 volume fluxes per unit surface (in mm^3 s^{-1} cm^{-2}) as determined with Eq. (28), desorbing from a flute and a coupe, respectively, filled with 100 mL of champagne, all along the first 10 min following the pouring process.

the champagne free surface, a parameter useful for champagne tasting, will be achieved by the use of gas microchromatography in a near future.

B. The role of temperature

In order to test the influence of champagne temperature on the kinetics of CO_2 release from a flute, experiments were performed at three sets of champagne temperature: 4, 12, and 20 °C, respectively, in a temperature-controlled room (Liger-Belair *et al.*, 2009b). The total CO_2 volume fluxes outgassing from the flute poured with champagne, during the first 10 min following pouring and for each champagne temperature, are presented in the graph displayed in Fig. 1.28. Experimentally, it is clear that the lower the champagne temperature, the lower CO_2 volume fluxes outgassing from the flute and especially in the early moments following the pouring process.

As in the preceding paragraph, correlations between CO_2 volume fluxes outgassing from the flute and dissolved CO_2 concentrations in champagne were done. They are displayed in Fig. 1.29, for each

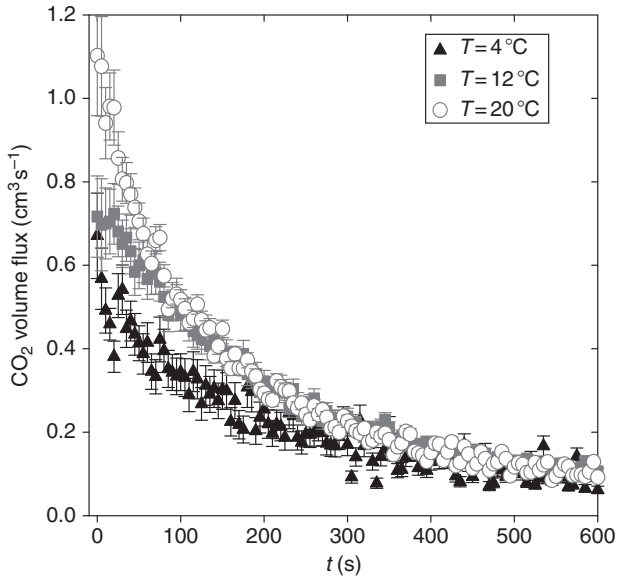

FIGURE 1.28 CO_2 volume fluxes recordings (in $cm^3\ s^{-1}$) desorbing from a 100-mL flute poured with champagne, all along the first 10 min following the pouring process, and at three different champagne temperatures; each datum of each time series is the arithmetic average of six successive values recorded from six successive pourings; standard deviations correspond to the root-mean-square deviations of the values provided by the six successive data recordings.

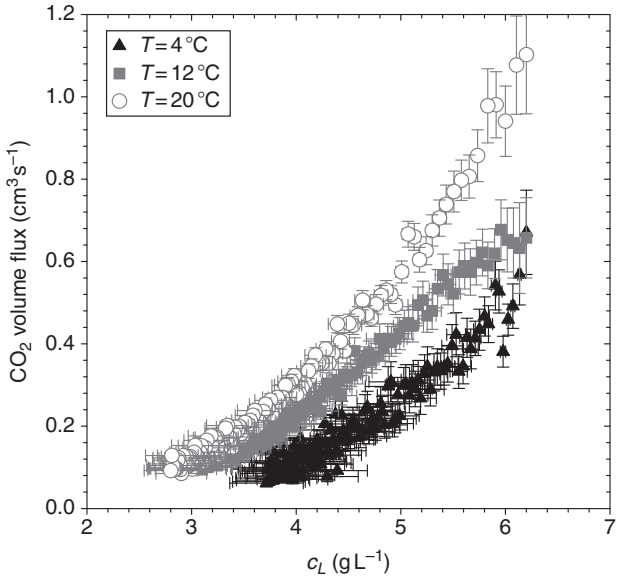

FIGURE 1.29 CO_2 volume fluxes recordings (in $cm^3\ s^{-1}$) desorbing from a 100-mL flute poured with champagne as a function of its dissolved-CO_2 concentration, and at three different champagne temperatures.

champagne temperature. It is clear from Fig. 1.29 that, for a given dissolved CO_2 concentration of champagne, the lower the champagne temperature, the lower CO_2 volume fluxes outgassing from the flute.

VI. CLOSE-UP ON BUBBLES BURSTING AT THE LIQUID SURFACE

A. The bursting process as frozen by high-speed photography

A champagne bubble reaches the liquid surface with a size that depends on the distance h traveled from its nucleation site, as expressed in Eq. (27). Experimentally, it was observed that bubble diameters rarely exceed about 1 mm. At the free surface, the shape of a bubble results from a balance between two opposing effects: the buoyancy F_B, of order of $\rho g \pi R^3$, which tends to make it emerge from the liquid surface and a capillary force F_C inside the hemispherical thin liquid film, of the order of $\sigma \pi R$, which tends to maintain the bubble below the liquid surface. In the case of champagne millimetric bubbles, buoyancy can be neglected in comparison to capillary effects. Consequently, like a tiny iceberg, a bubble only slightly emerges from the liquid surface, with most of its volume

remaining below the free surface. The emerged part of the bubble, the bubble-cap, is essentially a spherically shaped film of liquid, which gets thinner and thinner as the liquid drains back into the liquid bulk. A bubble-cap which has reached a critical thickness of about 100 nm becomes so thin and sensitive to such disturbances as vibrations and temperature change that it finally ruptures (Liger-Belair *et al.*, 2001a). For bubbles of millimeter size, the disintegration of the bubble-cap takes from 10 to 100 μs. During this extremely brief initial phase, the bulk shape of the bubble is literally ''frozen'', and a nearly millimetric open cavity remains as a tiny indentation in the liquid surface (see the high-speed photograph displayed in Fig. 1.30).

Then, a complex hydrodynamic process ensues, causing the collapse of the submerged part of the bubble and projecting into the air a liquid jet which quickly breaks up into tiny droplets of liquid (called jet drops). This process is indeed characteristic of every carbonated beverage. Generally speaking, the number, size, and velocity of jet drops produced during bubble collapse depend on the size of the initial bursting bubble (Spiel *et al.*, 1994, 1995, 1997, 1998). In Fig. 1.31, the close-up high-speed photograph of a tiny liquid jet caused by the collapse of a champagne bubble is displayed (Liger-Belair *et al.*, 2001a).

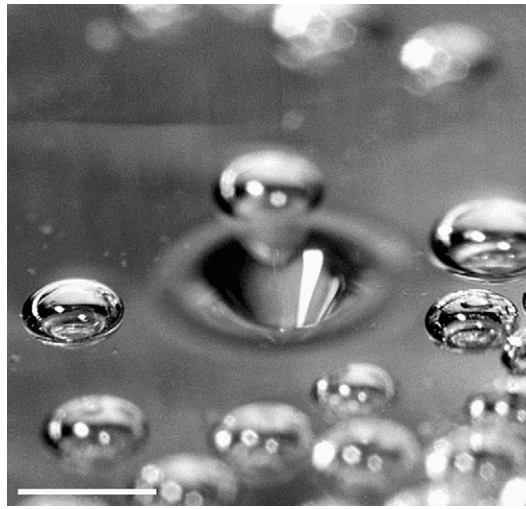

FIGURE 1.30 The bubble-cap of a bubble at the champagne surface has just ruptured (on a time scale of 10–100 μs); during this extremely brief initial phase, the bulk shape of the bubble has been "frozen," and a nearly millimetric open cavity remains as a tiny indentation in the liquid surface (bar = 1 mm; photograph by Gérard Liger-Belair).

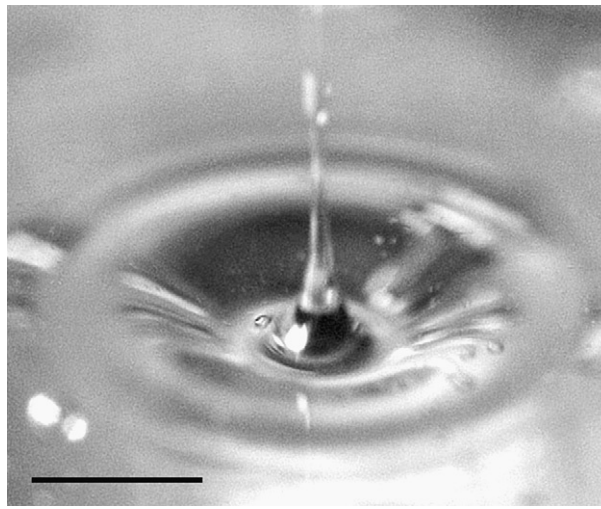

FIGURE 1.31 The collapsing bubble cavity gives rise to a high-speed liquid jet above the champagne surface (bar = 1 mm; photograph by Gérard Liger-Belair).

B. A paternoster for surface active molecules

As champagne or sparkling wine is poured into a glass, the myriad of ascending bubbles collapses and therefore radiates a multitude of tiny droplets above the free surface, into the form of very characteristic and refreshing aerosols, as shown in the photograph displayed in Fig. 1.32. Those tiny droplets ejected up to several centimeters above the liquid surface, partly evaporate themselves, thus accelerating the transfer of the numerous aromatic volatile organic compounds above the liquid surface. This very characteristic fizz considerably enhances the flavor release in comparison with that from a flat wine, for example. Laser tomography techniques were applied to freeze the huge number of bursting events and the myriad of droplets ejected above champagne glasses in real consuming conditions (see the tomography of the droplets' cloud above the surface of a coupe displayed in Fig. 1.33; Liger-Belair *et al.*, 2008).

Moreover, based on a phenomenological analogy between the fizz of the ocean and the fizz in Champagne wines, it was hypothesized a few years ago, that aerosols found in the headspace above a glass poured with champagne could considerably enhance the fragrance release of champagne by bringing chemical compounds to the taster's nostrils, showing both surface activity and organoleptic interest (Liger-Belair *et al.*, 2001a). Very recently, ultra high resolution mass spectrometry was used in order to analyze the aerosols released by champagne bubbles (Liger-Belair *et al.*, 2009a). Compared with the liquid bulk in the glass itself, the aerosols

FIGURE 1.32 The collapse of hundreds of bubbles at the free surface radiates a cloud of tiny droplets which is characteristic of champagne and other sparkling wines and which complements the sensual experience of the taster (©Alain Cornu/Collection CIVC).

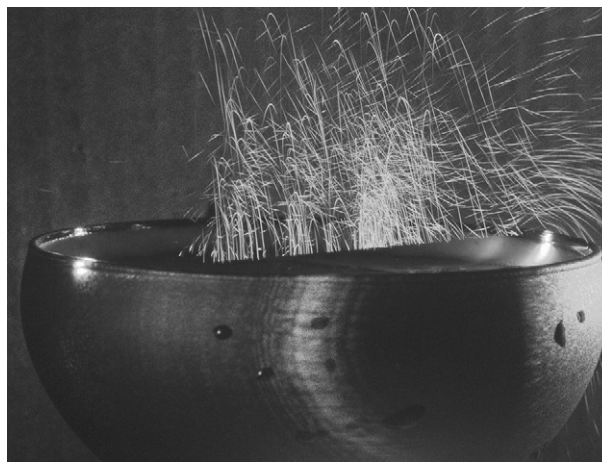

FIGURE 1.33 The cloud constituted by myriads of tiny droplets ejected from bubbles' bursting above the surface of a coupe, as seen through laser tomography technique; the droplets' trajectories are materialized by blue streaks of light during the 1 s-exposure time of a digital photo camera (photograph by G. Liger-Belair, F. Beaumont, and G. Polidori).

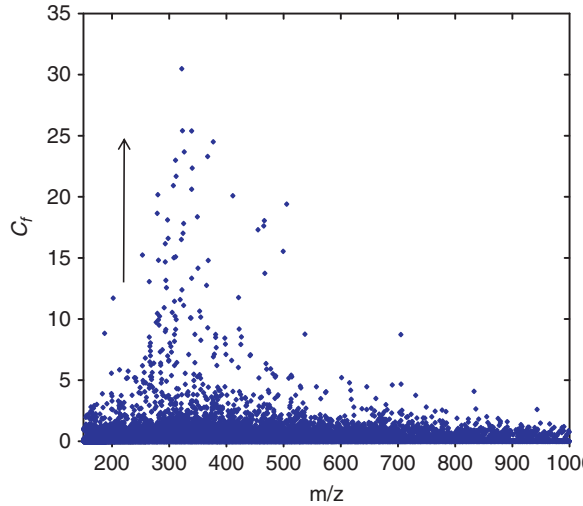

FIGURE 1.34 Concentration factors analysis of all masses present in the mass spectra of champagne aerosols and bulk, respectively (in the whole mass range *m/z* 150–1000).

contained an overconcentration of compounds known to be aromatic or the precursors of aromas (see Fig. 1.34). Each dot displayed in Fig. 1.34 represents the concentration factor of a given compound found in the aerosols (i.e., the ratio of its concentration in the aerosols to its concentration in the bulk, below the champagne surface). These compounds, mostly including saturated and unsaturated fatty acids, act as surfactants (i.e., as double-ended compounds with one end attracted to the liquid phase and another that shuns it). It was suggested that champagne bubbles drain these compounds out of the liquid bulk toward the liquid surface, with the hydrophobic end attracted by the bubble's airy inside and the hydrophilic end attracted by the liquid outside. The bubbles then rise to the surface of the glass where they pop, releasing the compounds as aerosols.

A detailed scheme of this mechanism is displayed in Fig. 1.35, together with high-speed photographs of the bursting process. This recent discovery supports the idea that rising and collapsing bubbles act as a continuous paternoster lift for aromas in every glass of champagne. Aerosols were thus found to hold the organoleptic ''essence'' of champagne.

C. When champagne bubbles dress up like flowers

The close observation of bubbles collapsing at the free surface of a glass poured with champagne also revealed another unexpected and lovely phenomenon. A few seconds after pouring, and after the collapse of the

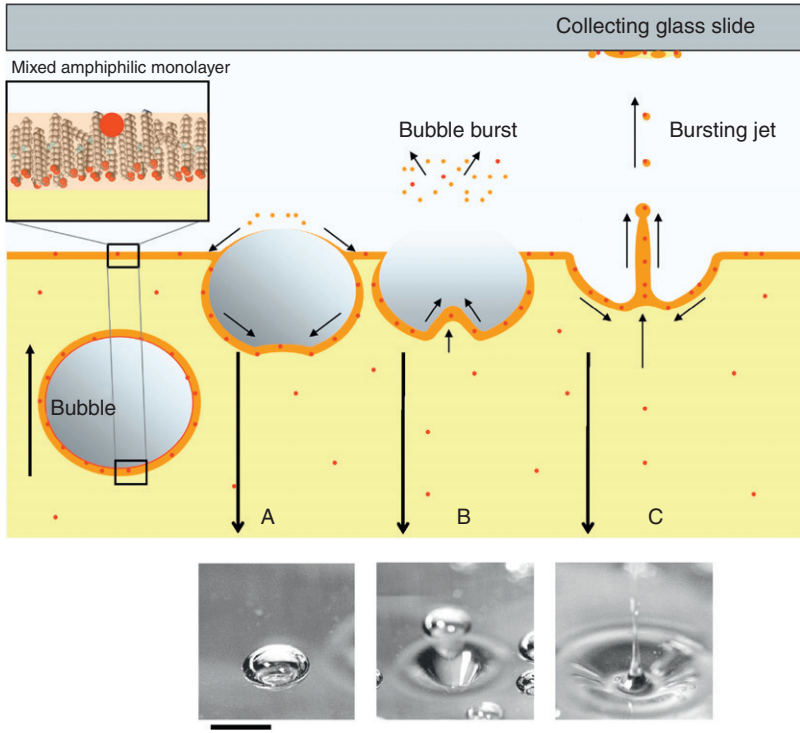

FIGURE 1.35 Scheme of the "bubble bursting" mechanism responsible for the ejection of champagne aerosols overconcentrated with compounds showing both surface activity and aromatic properties (these compounds appear as red dots); below are displayed high-speed photographs of a bubble collapse, leading to the projection of a liquid jet which quickly breaks up into tiny droplets (bar = 1 mm).

foamy head, the surface of a champagne flute is covered with a layer of bubbles—a kind of bubble raft, also called bidimensional foam, where each bubble is generally surrounded by six neighboring bubbles (see Fig. 1.36).

Scientifically speaking, bubbles arrange themselves in an approximate hexagonal pattern, strikingly resembling those in beeswax. While snapping pictures of the bubble raft after pouring, Liger-Belair also accidentally took some pictures of bubbles collapsing close to one another in the raft. When the bubble-cap of a bubble ruptures and leaves an open cavity at the free surface, adjacent bubble-caps are sucked toward this empty cavity and create unexpected and short-lived flower-shaped structures, unfortunately invisible to the naked eye (see the high-speed photograph displayed in Fig. 1.37; Liger-Belair *et al.*, 2001b; Liger-Belair and Jeandet, 2003). Shear stresses induced by bubbles trapped in the close vicinity of a

FIGURE 1.36 A few seconds after pouring, and after the collapse of the foamy head, the surface of a champagne flute is covered with a layer of quite monodisperse millimetric bubbles, where bubbles arrange themselves in an approximate hexagonal pattern, strikingly resembling those in beeswax (photograph by Gérard Liger-Belair).

FIGURE 1.37 Flower-shaped structure found during the collapse of bubbles in the bubble raft at the free surface of a flute poured with champagne (bar $=$ 1 cm; photograph by Gérard Liger-Belair).

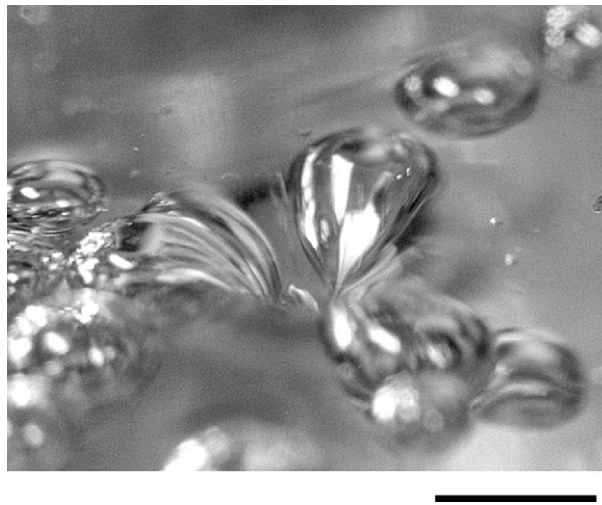

FIGURE 1.38 Shear stresses experienced by bubbles adjacent to a collapsing one at the free surface of a flute poured with champagne (bar = 1 cm; photograph by Gérard Liger-Belair).

collapsing one are even better visualized on the high-speed photograph displayed in Fig. 1.38, where the bubble raft is not complete. Such behavior first appeared counter intuitive to me. Paradoxically, adjacent bubble-caps are sucked and not blown-up by bursting bubbles, contrary to what could have been expected at first glance.

Actually, after the disintegration of a bubble-cap, the hexagonal symmetry around adjoining bubbles is suddenly locally broken. Therefore, the symmetry in the field of capillary pressure around adjoining bubbles is also locally broken. Capillary pressure gradients all around the now empty cavity are detailed in Fig. 1.39. Signs $\pm$ indicate a pressure above/below the atmospheric pressure P_0. Finally, inertia and gravity being neglected, the full Navier–Stokes equation applied to the fluid within the thin liquid film of adjoining bubble-caps drawn by capillary pressure gradients, reduces itself to a simple balance between the capillary pressure gradients and the viscous dissipation as follows:

$$\eta\left(\Delta\vec{u}\right)_S = \left(\vec{\nabla}P\right)_S \tag{29}$$

where u is the velocity in the thin liquid film of adjacent bubble-caps, η is the champagne viscosity, $\vec{\nabla}P$ are the capillary pressure gradients, and S being the axial coordinate which follows the bubble-cap's curvature and along which the fluid within the thin film is displaced.

The asymmetry in the capillary pressure gradients distribution around a bubble-cap adjacent to an empty cavity is supposed to be the main

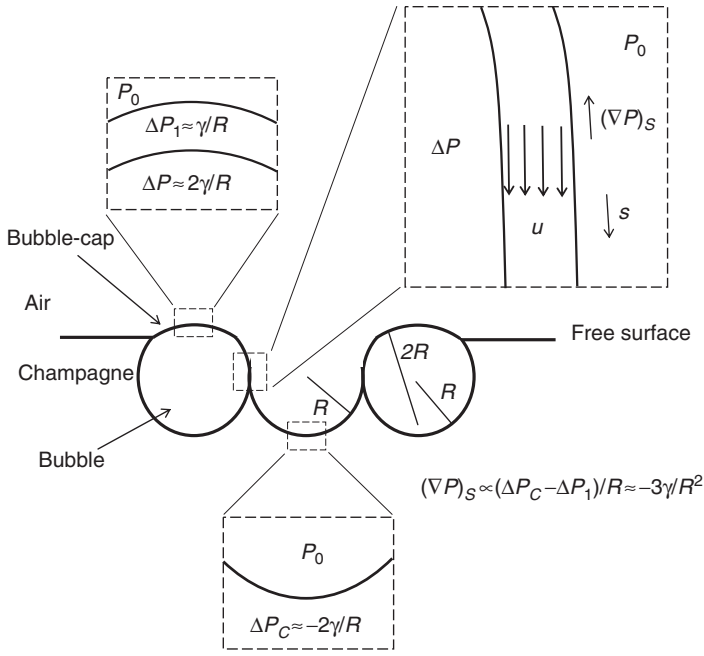

FIGURE 1.39 Schematic transversal representation of the situation, as frozen after the disintegration of the central bubble-cap.

driving force of the violent sucking process experienced by a bubble-cap in touch with a bursting bubble. Actually, due to higher capillary pressure gradients, the liquid flows that develop in the half part of the bubble-cap close to the open cavity are thus expected to be higher than those which develop in the rest of the bubble-cap. It ensues a violent stretching of adjoining bubble-caps toward the now empty cavity, which is clearly visible on the photographs displayed in Figs. 1.37 and 1.38. More recently, those flower-shaped structures have been observed during the coarsening of bidimensional aqueous foams, obtained by mixing a surfactant, sodium dodecyl sulphate (SDS), with pure water (Ritacco *et al.*, 2007). But it is worth noting that this lovely and short-lived process was first observed at the top of a champagne flute.

D. Avalanches of bursting events in the bubble raft?

Actually, avalanches of popping bubbles were put in evidence during the coarsening of bidimensional and three-dimensional aqueous foams (Ritacco *et al.*, 2007; Vandewalle *et al.*, 2001). How does the bubble raft behave at the surface of a flute poured with champagne? Does a bursting

bubble produce a perturbation which extends to the neighboring bubbles and induce avalanches of bursting events which finally destroy the whole bubble raft? In the case of champagne wines, a few time sequences of bubbles bursting in the bubble raft have been captured with a high-speed video camera. One of them is displayed in Fig. 1.40.

Between Frame 1 and Frame 2, the bubble pointed with the black arrow has disappeared. In Frame 2, neighboring bubbles are literally sucked toward this now bubble-free area. Then, neighboring bubbles oscillate during a few milliseconds and progressively recover their initial hemispherical shape. In conclusion, in the case of bubbles adjacent to the collapsing ones, despite high shear stresses produced by a violent sucking process, bubbles adjacent to the collapsing ones were never found to

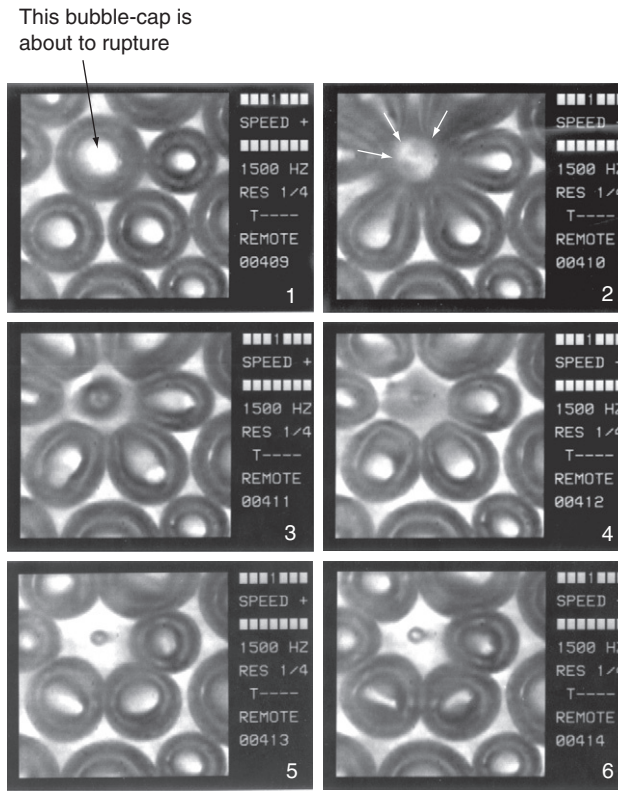

FIGURE 1.40 Time sequence illustrating the dynamics of adjoining bubbles in touch with a collapsing one at the free surface of flute poured with champagne; the whole process was filmed at 1500 frames/s; from frame 4, in the center of the empty cavity left by the collapsing bubble, a tiny air-bubble entrapment is observed (bar = 1 mm; photographs by Gérard Liger-Belair).

rupture and collapse in turn, thus causing a chain reaction. At the free surface of a flute poured with champagne, bursting events appear to be spatially and temporally noncorrelated. The absence of avalanches of bursting events seems to be linked to the champagne viscosity (which is about 50% higher than that of pure water; Ritacco *et al.*, 2007). It can also be noted that a tiny daughter bubble, approximately 10 times smaller than the initial central bubble, has been entrapped during the collapsing process of the central cavity (as clearly seen in Frames 3 and 4 of Fig. 1.40). Bubble entrapment during the collapsing process was already experimentally and numerically observed with single millimetric collapsing bubbles (Duchemin *et al.*, 2002; Herman and Mesler, 1987), including champagne bubbles (Liger-Belair *et al.*, 2001a).

ACKNOWLEDGMENTS

This research was partially supported by the Europol'Agro institute and by the Conseil Général de la Marne. Thanks are due to Champagne Moët & Chandon and Pommery for regularly supplying us with wine samples, and to Jean-Claude Colson and AROCU for encouraging and supporting our research. The author is also grateful to the CIVC for providing them with the photograph displayed in Fig. 1.1, and to Jacques Honvault for providing them with the photograph displayed in Fig. 1.5. Gérard Liger-Belair finally warmly thanks Clara Cilindre, Régis Gougeon and Philippe Schmitt-Kopplin for helpful discussions about the role played by bursting bubbles on the release of aromas.

REFERENCES

Agabaliantz, G. G. (1963). Bases scientifiques de la technologie des vins mousseux. *Bull. O.I.V.* **36**, 703–714.

Autret, G., Liger-Belair, G., Nuzillard, J.-M., Parmentier, M., Dubois de Montreynaud, A., Jeandet, P., Doan, B. T., and Beloeil, J.-C. (2005). Use of magnetic resonance spectroscopy for the investigation of the CO_2 dissolved in champagne and sparkling wines: A nondestructive and unintrusive method. *Anal. Chim. Acta.* **535**, 73–78.

De Gennes, P.-G., Brochard-Wyart, F., and Quéré, D. (2002). Gouttes, bulles, perles et ondes. Belin, Paris.

Duchemin, L., Popinet, S., Josserand, C., and Zaleski, S. (2002). Jet formation in bubbles bursting at a free surface. *Phys. Fluids* **14**, 3000–3008.

Dussaud, A. (1993). Etude des propriétés de surface statiques et dynamiques de solutions alcooliques de protéines: Application à la stabilité des mousses de boissons alcoolisées. Ph.D. Thesis, ENSIAA, Massy, France.

Herman, J. and Mesler, R. (1987). Bubble entrainment from bursting bubbles. *J. Colloid Interface Sci.* **117**, 565–569.

Jones, S. F., Evans, G. M., and Galvin, K. P. (1999). Bubble nucleation from gas cavities: A review. *Adv. Colloid Interface Sci.* **80**, 27–50.

Lide, D. R. and Frederikse, H. P. (1995). CRC Handbook of Chemistry and Physics. 76th edn. CRC Press, Boston.

Liger-Belair, G. (2002). Physicochemical approach to the effervescence in Champagne wines. *Ann. Phys. (Paris)* **27**, 1–106.

Liger-Belair, G. (2003). The science of bubbly. *Sci. Am.* **288**, 80–85.

Liger-Belair, G. (2004). Uncorked: The Science of Champagne. Princeton University Press, Princeton.

Liger-Belair, G. (2005). The physics and chemistry behind the bubbling properties of champagne and sparkling wines: A state-of-the-art review. *J. Agric. Food Chem.* **53**, 2788–2802.

Liger-Belair, G. (2006). Nucléation, ascension et éclatement d'une bulle de champagne. *Ann. Phys. (Paris)* **31**, 1–133.

Liger-Belair, G. (2009). Le Champagne: Effervescence! La science du champagne. Odile Jacob, Paris.

Liger-Belair, G. and Jeandet, P. (2003). Capillary-driven flower-shaped structures around bubbles collapsing in a bubble raft at the surface of a liquid of low viscosity. *Langmuir* **19**, 5771–5779.

Liger-Belair, G. and Rochard, J. (2008). Les vins effervescents, du terroir à la bulle. Dunod, Paris.

Liger-Belair, G., Lemaresquier, H., Robillard, B., Duteurtre, B., and Jeandet, P. (2001a). The secrets of fizz in champagne wines: A phenomenological study. *Am. J. Enol. Vitic.* **52**, 88–92.

Liger-Belair, G., Robillard, B., Vignes-Adler, M., and Jeandet, P. (2001b). Flower-shaped structures around bubbles collapsing in a bubble monolayer. *C. R. Phys.* **2**, 775–780.

Liger-Belair, G., Prost, E., Parmentier, M., Jeandet, P., and Nuzillard, J.-M. (2003). Diffusion coefficient of CO_2 molecules as determined by ^{13}C NMR in various carbonated beverages. *J. Agric. Food Chem.* **51**, 7560–7563.

Liger-Belair, G., Topgaard, D., Voisin, C., and Jeandet, P. (2004). Is the wall of a cellulose fiber saturated with liquid whether or not permeable with CO_2 dissolved molecules: Application to bubble nucleation in champagne wines. *Langmuir* **20**, 4132–4138.

Liger-Belair, G., Tufaile, A., Robillard, B., Jeandet, P., and Sartorelli, J.-C. (2005a). Period-adding route in sparkling bubbles. *Phys. Rev. E* **72**, 037204.

Liger-Belair, G., Voisin, C., and Jeandet, P. (2005b). Modeling non-classical heterogeneous bubble nucleation from cellulose fibers: Applications to bubbling in carbonated beverages. *J. Phys. Chem. B* **109**, 14573–14580.

Liger-Belair, G., Parmentier, M., and Jeandet, P. (2006a). Modeling the kinetics of bubble nucleation in champagne and carbonated beverages. *J. Phys. Chem. B* **110**, 21145–21151.

Liger-Belair, G., Tufaile, A., Jeandet, P., and Sartorelli, J.-C. (2006b). Champagne experiences various rhythmical bubbling regimes in a flute. *J. Agric. Food. Chem.* **54**, 6989–6995.

Liger-Belair, G., Religieux, J.-B., Fohanno, S., Vialatte, M.-A., Jeandet, P., and Polidori, G. (2007). Visualization of mixing flow phenomena in champagne glasses under various glass-shape and engravement conditions. *J. Agric. Food Chem.* **55**, 882–888.

Liger-Belair, G., Polidori, G., and Jeandet, P. (2008). Recent advances in the science of champagne bubbles. *Chem. Soc. Rev.* **37**, 2490–2511.

Liger-Belair, G., Cilindre, C., Gougeon, R., Lucio, M., Gebefügi, I., Jeandet, P., and Schmitt-Kopplin, P. (2009a). Unraveling different chemical fingerprints between a champagne wine and its aerosols. *Proc. Natl. Acad. Sci. USA* **106**, 16545–16549.

Liger-Belair, G., Villaume, S., Cilindre, C., and Jeandet, P. (2009b). Kinetics of CO_2 fluxes outgassing from champagne glasses in tasting conditions: The role of temperature. *J. Agric. Food Chem.* **57**, 1997–2003.

Liger-Belair, G., Villaume, S., Cilindre, C., Polidori, G., and Jeandet, P. (2009c). CO_2 volume fluxes outgassing from champagne glasses in tasting conditions: Flute versus coupe. *J. Agric. Food Chem.* **57**, 4939–4947.

Lubetkin, S. D. (2003). Why is it much easier to nucleate gas bubbles than theory predicts? *Langmuir* **19**, 2575–2587.

Lubetkin, S. D. and Blackwell, M. (1988). The nucleation of bubbles in supersaturated solutions. *J. Colloid Interface Sci.* **126**, 610–615.

Lugli, F. and Zerbetto, F. (2007). An introduction to bubble dynamics. *Phys. Chem. Chem. Phys.* **9**, 2447–2456.

Lynch, D. M. and Bamforth, C. W. (2002). Measurement and characterisation of bubble nucleation in beer. *J. Food. Sci.* **67**, 2696–2701.

O'Sullivan, A. (1997). Cellulose: The structure slowly unravels. *Cellulose* **4**, 173–207.

Polidori, G., Beaumont, F., Jeandet, P., and Liger-Belair, G. (2008). Visualization of swirling flows in champagne glasses. *J. Visual.* **11**, 184.

Priser, C., Etievant, P. X., Nicklaus, S., and Brun, O. (1997). Representative champagne wine extracts for gas chromatography olfactometry analysis. *J. Agric. Food Chem.* **45**, 3511–3514.

Ritacco, H., Kiefer, F., and Langevin, D. (2007). Lifetime of bubble rafts: Cooperativity and avalanches. *Phys. Rev. Lett.* **98**, 244501.

Ronteltap, A. D., Hollemans, M., Bisperink, C. G., and Prins, A. (1991). Beer foam physics. *Master Brew. Ass. Am. Tech. Quart.* **28**, 25–32.

Shafer, N. E. and Zare, R. N. (1991). Through a beer glass darkly. *Phys. Today* **44**, 48–52.

Spiel, D. E. (1994). The number and size of jet drops produced by air bubbles bursting on a fresh water surface. *J. Geophys. Res.* **99**, 10289–10296.

Spiel, D. E. (1995). On the birth of jet drops from bubbles bursting on water surfaces. *J. Geophys. Res.* **100**, 4995–5006.

Spiel, D. E. (1997). More on the births of jet drops from bubbles bursting on seawater surfaces. *J. Geophys. Res.* **102**, 5815–5821.

Spiel, D. E. (1998). On the birth of film drops from bubbles bursting on seawater surfaces. *J. Geophys. Res.* **103**, 24907–24918.

Tominaga, T., Guimbertau, G., and Dubourdieu, D. (2003). Role of certain volatile thiols in the bouquet of aged Champagne wines. *J. Agric. Food Chem.* **51**, 1016–1020.

Topgaard, D. (2003). Nuclear Magnetic Resonance Studies of Water Self-diffusion in Porous System. Ph.D. thesis, Lund University, Sweden.

Vandewalle, N., Lentz, J.-F., Dorbolo, S., and Brisbois, F. (2001). Avalanches of popping bubbles in collapsing foams. *Phys. Rev. Lett.* **86**, 179–182.

Zhang, Y. and Xu, Z. (2008). Fizzics of bubble growth in beer and champagne. *Elements* **4**, 47–49.